# Destabilization of buried carbon under changing moisture regimes

Manisha Dolui[1†], Teneille Nel[1*†], Abbygail R. McMurtry[2], Stephanie Chacon[1], Joseph A. Mason[3], Laura M. Phillips[2], Erika Marin-Spiotta[3], Marie-Anne de Graaff[2], Asmeret Asefaw Berhe[1], Teamrat A. Ghezzehei[1]

[1*]Department of Life and Environmental Sciences, University of California, Merced, 5200 Lake Rd, Merced, California, 95343, United States.
[2]Department of Geography, University of Wisconsin-Madison, 550 North Park Street, Madison, Wisconsin, 53706, United States.
[3]Department of Biological Sciences, Boise State University, 1910 University Drive, Boise, Idaho, 83725, United States.

*Corresponding author(s). E-mail(s): teneille.nel@gmail.com;
†These authors contributed equally to this work.

**Abstract**

Paleosols formed by the burial of topsoil during landscape evolution can sequester substantial amounts of soil organic carbon (SOC) over millennia due to protection from surface disturbances. We investigated the moisture sensitivity of buried SOC storage in the Brady paleosol, a loess-derived soil in Nebraska, USA, where historical aeolian deposition during the Pleistocene–Holocene transition buried soils up to 6 m deep. Topsoils from erosional (up to 1.8 m depth) and depositional (up to 5.8 m depth) transects were incubated under two moisture regimes - continuous wetting (60% water-holding capacity) and repeated drying–rewetting - to assess soil organic matter (SOM) vulnerability to changing hydrologic conditions. SOC decomposition rates modeled from $CO_2$ fluxes were consistently higher in erosional than depositional settings, with surface re-exposure of Brady soils enhancing microbial accessibility and destabilization. A two-pool model showed that >96% of SOC was stored in a slow-cycling pool, particularly in deeply buried soils where stabilization was linked to mineral association, fine particles, and Ca-mediated flocculation. However, this pool decomposed more rapidly in

shallower Brady soils (higher turnover rate relative to buried soil), reflecting increased microbial responsiveness to surface-driven processes.
Drying–rewetting cycles caused greater C losses from Brady soils than continuous wetting, despite the dominance of the slow pool and depletion of labile C. These cycles also accelerated fast pool decay in modern soils and erosional transects, whereas burial dampened variability in Brady soils. Although continuous wetting increased overall decay in burial transects during the incubation period, wet–dry cycles destabilized the slow pool, which may result in greater long-term C loss. Together, these results underscore the importance of burial depth, geomorphic context, and moisture regime in shaping the long-term vulnerability of ancient SOC under climate change.

**Keywords:** paleosol, erosion, soil carbon stabilization, organic matter decomposition

# 1 Introduction

Global temperatures have risen by 1°C since the industrial era due to anthropogenic $CO_2$ emissions, confirming human-driven climate change (IPCC 2018). Alongside warming, precipitation regimes are shifting - marked by increased frequency and intensity of wetting and drying events, especially in more arid ecosystems. These hydrologic fluctuations can destabilize long-stored soil organic carbon (SOC) by disrupting aggregates, increasing dissolution and solute mobility, and stimulating microbial decomposition (Berhe et al. 2012; Min et al. 2020; Hicks Pries et al. 2023). While limiting warming to below 2°C remains critical, mitigation via emissions reductions alone may be insufficient. Preserving or enhancing terrestrial carbon sinks, especially soils, offers a complementary pathway for climate stabilization.

Soil organic matter (SOM) encompasses the full suite of organic compounds in soil, including living biomass, particulate debris, and mineral-associated organic molecules. SOC refers specifically to the carbon fraction of SOM and is the metric used throughout this study to quantify carbon stocks and fluxes. While many studies examine topsoil carbon dynamics, whole-soil responses to changes in climate have rarely been tested (Hicks Pries et al. 2017). Subsoils hold nearly half of global SOC stocks (Jobbagy and Jackson 2000) and this deep-soil carbon may be more sensitive to varying environmental conditions than surface soil (Min et al. 2020). Organic inputs reach subsoils via leaching of dissolved organic carbon and vertical transport of litter by bioturbation. SOC in deeper horizons typically features low carbon to nitrogen (C:N) ratios and long mean residence times, suggesting advanced microbial processing and relative stability (Rumpel and Kögel-Knabner 2011). In contrast, topsoils buried by aeolian or alluvial deposition often retain legacy carbon signatures reflecting past vegetation and climate (Marin-Spiotta et al. 2014), diverging from modern surface soils. These buried soils have historically been isolated from near-surface conditions, including temperature and moisture fluctuations. Previous research supports this isolation effect: for instance, Chaopricha (2013) found negligible $CO_2$ fluxes from Brady Soil collected from 4 m below the modern surface when no water was added, indicating extremely limited microbial activity under such dry, oxygen-poor conditions.

The stability of buried SOC, however, depends entirely on continued isolation from surface conditions – an assumption increasingly at odds with landscape dynamics across the Great Plains. Accelerated gully erosion, agricultural tillage, and more intense precipitation events are progressively exhuming paleosols that remained protected for millennia (Mason et al. 2008; Jacobs and Mason 2007). Yet the decomposition response of this ancient carbon to re-exposure remains poorly constrained. Will millennia-old SOC decompose rapidly once oxygen and moisture access is restored, or do the same properties that enabled its long-term preservation – fine texture, mineral associations, chemical recalcitrance – confer lasting resistance? This uncertainty carries substantial implications for carbon-climate feedbacks: if re-exposed paleosol carbon proves vulnerable to decomposition, ongoing erosion across loess landscapes could convert a long-term carbon sink into an unaccounted source.

Subsurface environments typically have limited oxygen, C inputs, and water availability, all of which constrain microbial activity and promote long-term SOC persistence (Soong et al. 2021). However, this protection may be compromised under climate change scenarios involving increased rainfall, warming, and surface disturbance (Fontaine et al. 2007; Gao et al. 2020; Hicks Pries et al. 2023). While burial isolates SOM from decomposers, enhancing its stability (Berhe et al. 2007; Stacy et al. 2015; Berhe et al. 2008), soil erosion, root intrusion, and hydrologic shifts can re-expose previously protected SOM. Erosion may also replace eroded C with increased photosynthate additions due to rejuvenation of rock-derived nutrients (Berhe et al. 2018). Given the global extent of geomorphic disturbance and the potential for reactivated decomposition, buried soils may represent an extensive but under-characterized carbon pool whose long-term persistence is uncertain (Chaopricha and Marín-Spiotta 2014; Szymanski 2021; Pal et al. 2023).

SOM decomposition is mediated by geomorphic and geochemical controls. Soil texture, mineralogy, and ionic composition shape organo-mineral associations and influence microbial access. Thermal transformation of buried SOM into condensed aromatic compounds can also increase resistance to decomposition (Marin-Spiotta et al. 2011; Schmidt et al. 2011). Recent findings from Dolui et al. (in press) link persistent SOM turnover in buried soils to fine textures, higher conductivity, and enhanced organo-mineral bonding. These stabilizing mechanisms weaken with erosional exposure to surface conditions (soil moisture and oxygen) and priming of previously-stable SOM due to the introduction of fresh organic matter inputs (McMurtry et al. 2024), making SOM more vulnerable to loss.

Soil moisture dynamics are central to SOM persistence. Wetting and drying–rewetting cycles can destabilize aggregates, increase dissolved organic carbon leaching, and stimulate mineral-associated OM loss (Berhe et al. 2012; Neff and Asner 2001; Li et al. 2023). Moisture influences microbial processes by modulating water potential, oxygen diffusion, and solute transport (Chowdhury et al. 2011; Davidson et al. 2012). Texture controls water retention during drying, while aggregate structure governs accessibility under saturated conditions (Or and Tuller 1999; Ghezzehei et al. 2019).

In surface soils, especially in semi-arid and Mediterranean systems, drying–rewetting cycles produce strong mineralization pulses (Miller et al. 2005; Zhu and

Cheng 2013). Such cycles break down aggregates and release labile SOM, stimulating priming effects (Najera et al. 2020). Soils with broader pore-size distributions may retain water longer, sustaining microbial activity and potentially increasing cumulative SOM loss (Goebel et al. 2005). The effects of increased rainfall also depend on seasonal timing; for instance, winter precipitation can enhance subsoil C storage more than spring rain due to deeper translocation of carbon (Wahab et al. 2025).

As soils dry, physical and chemical processes can strengthen OM–mineral interactions. Solute precipitation, matric tension, and shifts toward stronger bonding (e.g., inner-sphere complexes) promote greater SOM–mineral affinity (Kaiser et al. 2015; Kemper et al. 1987; Kang and Xing 2008). Reorientation of amphiphilic compounds on mineral surfaces can increase hydrophobicity (Horne and McIntosh 2000), potentially misleading assessments of SOM stability under drier conditions.

$CO_2$ efflux in subsoils is shaped by physical constraints - lower porosity, higher bulk density, and greater water-filled pore space - which suppress microbial respiration after rewetting (Min et al. 2020; Hill et al. 1985; Beare et al. 2009; Schrumpf et al. 2013). Subsurface microbial communities are often dominated by drought-tolerant fungi (Bird and Torn 2006), and experience fewer moisture and temperature fluctuations than surface soils (Rumpel and Kögel-Knabner 2011). Microbial "resistance" to drying manifests as reduced respiration during dry-down, while "resilience" describes rapid respiration rebound after rewetting (Leizeaga et al. 2021; Griffiths and Philippot 2013). Soils with frequent drying–rewetting history tend to support more resilient microbial communities (Fierer and Schimel 2003; Steenwerth et al. 2005).

In semi-arid systems, soil inorganic carbon (SIC) also contributes to carbon dynamics. SIC accumulates at depth through carbonate dissolution–precipitation cycles (Sharififar et al. 2023; Batool et al. 2024; Cotrufo and Lavallee 2025). This is seen in the Brady Soil, a late Pleistocene paleosol buried by loess ca. 13,000–10,000 years ago in the Great Plains of the US (Jacobs and Mason 2007; McDowell 2020). SIC interacts with SOC via aggregation and mineral associations but can be mobilized through leaching under increased moisture conditions (Naorem et al. 2022; Liu et al. 2018; Tsypin and Macpherson 2012).

Despite growing interest in buried SOM, moisture-driven decomposition patterns across landforms remain unclear. This study investigates the sensitivity of modern and buried SOM to moisture inputs under erosional and depositional geomorphic conditions in the Brady Soil. According to the U.S. National Climate Assessment (2018), the Central Great Plains region of Nebraska is projected to warm by 3.5–9.5°C, with annual precipitation increasing by  2.5 cm. Erosion driven by agriculture, grazing, wind, and rainfall threatens to re-expose buried SOM to surface conditions.

We conducted a laboratory incubation using soils collected near Wauneta, Nebraska, to compare $CO_2$ efflux under continuous wetting versus drying–rewetting regimes. The area's semi-arid climate with seasonal moisture variability provides a relevant setting to test SOM responses to hydrologic fluctuations. Our hypotheses were: (i) Brady SOM is more stable and decomposes more slowly than modern SOM as reduced moisture and oxygen availability limit decomposition of SOM due to isolation from the soil surface; (ii) buried SOM in erosional settings is more vulnerable

to loss due to exposure of previously protected SOM to surface conditions and mixing with modern carbon; and (iii) wetting will stimulate $CO_2$ release from previously buried soils as a result of increased substrate availability due to enhanced dissolution, solute transport, microbial decomposition, and/or aggregate disruption. By evaluating the interactions between moisture, geomorphology, and SOM dynamics, we aim to improve predictions of carbon stability under future climate and land-use change.

# 2 Methods and materials

## 2.1 Site and sampling

The field site is situated near Wauneta, within the loess tablelands of southeastern Nebraska, USA (40°29'52.8" N, 101°24'36" W; see Fig. 1). The region experienced reduced loess input during the terminal Pleistocene and early Holocene (13–10 ka) that permitted soil formation, leading to the development of the Brady Soil. Subsequent aridification renewed dust flux, resulting in its burial by younger loess (Johnson et al. 2007; Mason et al. 2008). Additional loess accumulation throughout the Holocene preserved weaker paleosols formed during intermittent depositional pauses (Mason et al. 2003; Miao et al. 2007). Recognized as a key paleoenvironmental and stratigraphic unit, the Brady Soil is regionally traceable across Nebraska, northeastern Colorado, and northern Kansas (Johnson and Willey 2000).

The area is characterized by broad, flat uplands and sharply incised edges, providing natural windows into stratified soil profiles. Loess cover above the Brady Soil tapers in a downwind direction across the summits where it is thickest, producing burial transects of variable thickness. The local climate is semi-arid, with an average annual temperature of 9.7°C and ca. 495 mm of precipitation, concentrated during the summer months, with occasional snow in winter. Natural vegetation includes a mix of C3 and C4 grasses, replaced by cropland on many level surfaces today, but remaining at the study site and on steeper terrain in general.

Brady Soil exposures are visible in actively eroding margins, gullies, and roadside cuts. Prior investigations, including coring and field surveys, confirm its continuity beneath the summit landform (Jacobs and Mason 2004; Marin-Spiotta et al. 2014; Mason et al. 2008). Surface soils developed in Holocene loess are weakly developed and light-colored, typically classified as Mollisols, Inceptisols, or Entisols. Although different in age, modern and buried soils share similar parent material and mineralogy due to the region's limited weathering intensity. Brady A horizons (Ab) are identified by their dark grayish brown coloration (Munsell 10YR3/2 to 10YR4/2) and silt loam texture, generally overlying Bk or Bw horizons (Szymanski 2021; Jacobs and Mason 2007; McDowell 2020).

Sampling was conducted in 2016 and 2017 across two geomorphic settings: burial transects (where the Brady Soil is deeply buried beneath Holocene loess) and erosional transects (where the Brady Soil is exposed or shallowly buried due to hillslope erosion). Within each setting, three replicate transects were established. We collected samples at three depths relative to the soil surface from each of the transects per setting (details in Fig. 1). Sampling stratigraphy relative to the present land surface was categorized using Roman numerals (Supplementary Information, Table A1). At each

transect position, samples were collected from (1) the modern soil surface (0–30 cm), (2) the subsurface modern soil (30–60 cm, where present), and (3) the upper Brady paleosol horizon (0–30 cm into the Ab horizon, at variable depth below the modern surface depending on burial thickness). All samples were analyzed for physicochemical properties, but only samples from the 0-30 cm depth intervals were used for incubation experiments. Table A1 provides the specific sampling depths for each transect position. A Giddings probe (10.2 or 8.9 cm diameter) with plastic liners was used for intact sampling in burial settings, while soil pits were dug for erosional profiles. Complete methods are described in (Szymanski 2021).

## 2.2 Soil chemical and physical analyses

General soil physical and chemical properties were determined by standard soil analytical methods, as described in detail in Dolui et al. (2026) and Szymanski (2021). Briefly, soil pH and electrical conductivity (EC) of soil samples were determined in 1: 2 water extracts using a SevenExcellence multiparameter benchtop meter (Mettler Toledo, United States). Total carbon was determined by dry combustion using an ECS 4010 elemental combustion analyzer (Costech Analytical Technologies, Inc., USA); inorganic carbon was removed by acidification with 1M HCl prior to TOC determination. Exchangeable base cations ($Ca^{2+}$, $Mg^{2+}$, $Na^{+}$ and $K^{+}$) were were quantified by ICP-OES (Optima 5300 DV Spectrometer, Perkin-Elmer, Germany) following ammonium acetate extraction (buffered to pH 7). Sodium adsorption ratio (SAR) was determined by dividing concentration of Na in soil extract by the square root of half of sum of Ca and Mg concentrations (Dolui et al., in press). Particle size distribution was determined using the pipette method for clay (¡2 $\mu$m) and laser diffraction (Mastersizer 2000 particle size analyzer, Malvern Panalytical, UK) for silt and sand fractions. Radiocarbon ($^{14}C$) analyses of bulk soil samples were conducted to determine the age and turnover time of carbon in both modern and buried soils. Samples were pre-treated, combusted, and then measured by accelerator mass spectrometry using an FN accelerator mass spectrometer (Van de Graaff, US) at the center for accelerator mass spectrometry at Lawrence Livermore National Laboratory. The $\Delta^{14}C$ results were used in a homogeneous, open-system, steady-state soil carbon decomposition model to estimate carbon turnover times (Dolui et al. 2026) which were averaged for the three replicate transects.

## 2.3 Incubation experiments

The incubation experiment was set up to determine the effect of continuous wetting and drying–rewetting on SOC fluxes using soils that were collected from the upper layer of modern and Brady Soil samples at depositional and erosional transect types. To isolate the effects of moisture, roots >2 mm were removed by sieving and manual sorting. Samples from 0-30 cm depth from different transect numbers were homogenized (so that they had only unique paleostatus, transect type and burial/ erosional degree). Two types of water addition experiments were conducted: continuous wet and drying–rewetting. Two sub-samples were taken from each composite to perform biological replicates of each incubation experiment, such that there was a total number of 24 individual incubation vessels.

### 2.3.1 Experimental setup

The incubation experiments were conducted in 8 oz mason jars. Soil water holding capacity (WHC) was pre-determined by tensiometry (using pressure plates with an applied pressure of –33 kPa) and soil moisture content was monitored on a mass-basis by weighing soils weekly during the incubation. The treatments included (i) continuous wet – soils maintained at 60% WHC throughout the experiment and (ii) drying–rewetting cycles – soils were dried, then rewetted to 60% WHC. Treatment durations differed by experimental objective. The continuous wet incubation (225 days) was designed to capture the full trajectory of decomposition, enabling robust fitting of two-pool decay models that partition SOC into fast- and slow-cycling fractions. The wet-dry treatment (56 days, 8 cycles of 7-day drying followed by rewetting) was designed to assess cumulative effects of repeated moisture pulses over a timeframe comparable to a growing season. For direct comparison between treatments, we modeled $CO_2$ loss over equivalent 49-day windows and compared decay parameters derived from each treatment's full duration. Each treatment had two replicates (sub-samples derived from a single composite of replicate transects per soil type), and control soils were maintained at 5% WHC.

Previously homogenized soils were sub-sampled and added to jars at an equivalent of 30 ± 0.5 g dry mass. After adding a predetermined amount of ultra-pure Milli-Q water, the jars were kept at room temperature (ca. 25°C), matching the average summer soil temperature (when most precipitation occurs) at the site (UNL Soil Temperature Data). Jars were sealed with lids fitted with rubber septa for headspace gas collection, and silicone gel was applied around the septa to prevent gas leakage.

In the continuous wet experiment, soils were maintained at 60% WHC and sealed until sampling. On average, water loss was 0.01 mL/day, ranging from 0.005 to 0.02 mL/day. Water was added after gas sampling to avoid inducing the Birch effect. After each sampling, lids were left open for one hour to allow $CO_2$ equilibration with ambient air.

In the drying–rewetting experiment, soils were rewetted every 7 days by slowly adding Milli-Q water to reach 60% WHC. After water addition, jars were sealed, and headspace gas was sampled 6 hours later to capture Birch effect emissions. Soils were then dried to 5% WHC by removing the lids and incubating at ca. 25°C.

### 2.3.2 Sampling schedule and $CO_2$ analysis

In the continuous wet experiment, headspace gas samples for $CO_2$ analysis were collected on days 1, 3, 5, 7, 11, 16, 27, 55, 82, 114, 151, and 225. After each sampling, jar lids were opened for one hour to equilibrate with ambient air.

In the drying–rewetting experiment, jars were sealed for 6 hours after water addition, and headspace gas was sampled on days 1, 7, 21, 28, 35, 42, and 49 to evaluate the Birch effect. Control samples were collected on the same days for both experiments.

Evolved $CO_2$ concentrations were analyzed using a Shimadzu 2014 gas chromatograph (Kyoto, Japan) with a thermal conductivity detector at UC Merced and an LI-830 infrared gas analyzer (IRGA) at Lawrence Livermore National Laboratory (LLNL).

## 2.4 Statistical analyses

All statistical analyses were performed using CRAN-R 4.5.0 (R Core Team 2025). Soil-respired $CO_2$ measurements from incubation experiments were averaged across two biological replicates per treatment. Control samples were represented by single measurements due to sample constraints. Accordingly, statistical comparisons involving controls were interpreted with caution.

The concentration of soil-respired $CO_2$ was expressed as the mass of C respired per unit mass of SOC, calculated as:

$$\mu g\, C - CO_2\ g\ soil\ C^{-1} = mmol\, air * \frac{\mu mmol\ CO_2}{mol\ air} * \frac{10^{-3}\ mol\ air}{mmol\ air} * \frac{12\ \mu g\ C}{\mu mol\ C} * \frac{1}{g\ TOC} \tag{1}$$

For the continuously wet incubation, cumulative respiration was calculated by summing $CO_2$ fluxes over the 225-day experiment. Two-pool first-order decay models were fitted to cumulative respiration data according to:

$$C_{CO_2}(t) = C_0\left(1 - (f_f e^{-k_f t} + f_s e^{-k_s t})\right) \tag{2}$$

where $C_{CO_2}(t)$ is the cumulative mass of C ($\mu$g) respired by day $t$, $C_0$ denotes TOC, $f_f$ and $f_s$ represent the fast- and slow-cycling fractions of SOC (with $f_f + f_s = 1$), and $k_f$ and $k_s$ are the corresponding decay rate constants. Models were fitted using non-linear least-squares optimization with the `minpack.lm` package (Elzhov et al. 2023).

For the wet-dry cycling incubation, cumulative respiration was calculated by summing $CO_2$ fluxes over wetting periods only, assuming negligible respiration during drying phases (Chaopricha 2013). The effective incubation time ($t$) was approximated as the cumulative duration of wetting events (2 days over a 49-day experiment). Two-pool decay models were initially fitted following the same approach as for the continuously wet incubation.

Preliminary model fits indicated that the fast-cycling pool contributed negligibly to respiration during wet-dry cycling (slow:fast pool ratio $\sim$ 0.999:0.001), consistent with a functionally homogeneous system. Consequently, one-pool first-order decay models were also fitted for both incubation treatments:

$$C_{CO_2}(t) = C_0\left(1 - e^{-kt}\right) \tag{3}$$

where $k$ represents the single-pool decomposition rate constant.

The effects of transect type, paleostatus, degree of burial or exposure, and their interactions on SOM decomposition parameters (decay rates and pool sizes) were evaluated using linear mixed-effects models, treating biological replicates as a random effect (controls excluded). These analyses were conducted using the `nlme` (Pinheiro et al. 2024) and `emmeans` (Lenth 2024) packages. Significant differences among factor levels were assessed using pairwise Sidak-adjusted comparisons. For the wet–dry cycling experiment, similar models were applied to analyze day-1 $CO_2$ pulse responses.

Total $CO_2$ losses during wet-dry cycling (49 days) were compared to modeled $CO_2$ losses over an equivalent duration under continuous wetting using linear mixed-effects models with Paleostatus, transect type, and Depth as fixed effects and replicate as a random effect. Marginal means and pairwise comparisons were used to contrast incubation treatments. For control samples, Paleostatus and transect type were treated as fixed effects and Depth as a random effect. Despite limited replication, the large magnitude of difference between control and treatment fluxes (>45-fold) indicates that moisture addition, rather than incubation artifacts, drove observed respiration patterns.

Mean cumulative $CO_2$ losses between control and treatment groups were further compared using a Welch test following confirmation of unequal variances via a Bartlett test, implemented in the `stats` package (RStudio Team 2019). Linear mixed-effects models were also used to evaluate the effects of transect type and paleostatus on cumulative $CO_2$ losses in control samples, with Depth treated as a random effect.

Multiple linear regression (MLR) was used to quantify the influence of soil physicochemical properties (soil pH, EC, TOC and TIC contents, SAR, texture, and exchangeable base cations) on modeled SOM decomposition parameters. For the continuously wet incubation, MLR models were applied to fast- and slow-pool decay rates and slow-pool fraction sizes derived from two-pool models. For the wet–dry cycling incubation, MLR analyses were conducted on decomposition rates derived from one-pool models. Model selection followed stepwise forward and backward procedures, prioritizing parsimony based on Akaike Information Criterion (AIC) values using the `MASS` package (Venables and Ripley 2002). Model coefficients, intercepts, $R^2$, and root mean squared error (RMSE) were calculated using the `stats` package. Pairwise Pearson correlation matrices were generated to visualize relationships among soil properties and SOM decomposition parameters using the `stats` and `ggplot2` packages (RStudio Team 2019).

# 3 Results

## 3.1 General soil properties

The physicochemical properties of soils used in the incubation experiment are shown in Table 5. The soils were relatively alkaline (pH ranging from 6.89 to 7.77), especially the Brady Soil. The clay, silt and sand content placed the soils in the texture class category of silt loam. Total organic carbon was higher in modern soils due to active biomass inputs, while inorganic carbon content was higher in the Brady Soil due to carbonate formation (cite Dolui et al i.e. paper 1). The Brady soil of the burial transect was classified as saline (mean EC of 5.41 dS $m^{-1}$) and the CEC of soils was moderately high, ranging from 15.17 - 23.31 and indicating the presence of higher activity clays. The turnover time of bulk soils as derived from radiocarbon-based models, was much greater in the Brady Soil (8327 - 15 654 years) compared to modern soils (576.4 - 1451 years), confirming the long-term stability of SOM in the paleosol (cite Dolui et al. i.e., paper 1). The mean CN ratio in both Brady and modern soils was relatively low (ca. 10), indicating a sufficient supply of N for plant growth and microbial activity.

### 3.2 Effects of continuous wetting on soil $CO_2$ efflux

Cumulative C lost from soils via respiration of $CO_2$ during the continuously wet incubation are shown in Fig. 2. Raw incubation data and figures of merit of statistical comparative tests are available online at DOI: doi: 10.17632/fjw646gpyf.1.

In the continuous wet soil treatment group, modern soils evolved significantly higher $CO_2$ (mean of 30.6 mg $CO_2$-C g $C^{-1}$) compared to Brady Soil (mean of 15.9 $\pm$ 2.39 mg $CO_2$-C g $C^{-1}$) after 225 days of incubation ($p < 0.01$). Soils of the erosional transect type had greater cumulative C loss (mean of 29.3 mg $CO_2$-C g $C^{-1}$) compared to the depositional transect (mean of 17.3 $\pm$ 2.39 mg $CO_2$-C g $C^{-1}$, $p < 0.01$). However, the difference between cumulative C losses of erosional vs depositional transect types was not significant at the greatest depth.

Modern soil in the erosional transect had significantly higher cumulative C losses (mean of 35.9 mg $CO_2$-C g $C^{-1}$) than modern soil of the depositional transect (mean of 25.3 mg $CO_2$-C g $C^{-1}$, $p < 0.05$). Similarly, Brady Soil of the erosional transect had significantly higher cumulative C losses (mean of 22.6 mg $CO_2$-C g $C^{-1}$) compared to the depositional transect (mean of 9.28 mg $CO_2$-C g $C^{-1}$, $p < 0.05$).

The Brady soil with an intermediate degree of erosion had higher cumulative $CO_2$ loss (mean of 33.2 mg $CO_2$-C g $C^{-1}$) compared to Brady Soil of other depths, while the Brady soil with the greatest degree of burial had the lowest cumulative $CO_2$ loss (mean of 4.14 mg $CO_2$-C g $C^{-1}$, differences not significant). For Brady soil of the depositional transect, the magnitude of cumulative $CO_2$ efflux among different depths was in the order of shallowest > intermediate > deepest, whereas in the erosional transect, the order was intermediate > shallowest > deepest.

The cumulative $CO_2$ evolution of 60% WHC continuous wet experiments (mean of 23.3 mg $CO_2$-C g $C^{-1}$) was significantly greater than control soils maintained at 5% WHC (mean of 0.478 mg $CO_2$-C g $C^{-1}$, $p < 0.001$). Among the control soils, Brady Soil of the depositional transect had significantly greater C losses (mean of 0.561 mg $CO_2$-C g $C^{-1}$) compared to modern soils (mean of 0.253 $\pm$ 0.0683 mg $CO_2$-C g $C^{-1}$, $p < 0.05$), but C losses in modern and Brady Soil were more similar in the erosional transect (mean of 0.254 and 0.444 mg $CO_2$-C g $C^{-1}$ for modern and Brady Soil respectively, n.s.).

Significance of differences in cumulative $CO_2$ losses among degree of burial/ exposure for control samples could not be tested due to lack of replication, but we report observed differences. Among the depositional transect control soils, the shallowest depth Brady soil produced the greatest cumulative $CO_2$ loss, while modern soil collected from the intermediate degree of burial soil produced the least cumulative $CO_2$ loss. Among the erosional transect control soils, the most $CO_2$ was evolved in the intermediate depth Brady soils, and the lowest $CO_2$ was evolved in the modern soil collected from the lowest degree of burial.

### 3.3 Effect of drying and rewetting on soil $CO_2$ efflux

Daily C lost from soils via respiration of $CO_2$ during the dry-rewetting incubation are shown in Fig. A1 and cumulative C losses are shown in Fig. 3. Soil respiration data from the dry-rewetting incubation are available online at DOI: doi: 10.17632/fjw646gpyf.1.

The largest respiration fluxes were produced on the first day, with significantly greater cumulative $CO_2$ loss from modern soils (mean of 0.920 mg $CO_2$-C g $C^{-1}$) compared to Brady Soil (mean of 0.729 ± 0.034 mg $CO_2$-C g $C^{-1}$, $p < 0.01$), but the reverse was observed at the greatest depth. Respiration pulses declined over time for all soils. Control soils had a lower $day^{-1}$ pulse $CO_2$ (mean of 0.295 mg $CO_2$-C g $C^{-1}$) compared to the dry-rewetting treatment (mean of 0.824 mg $CO_2$-C g $C^{-1}$, $p < 0.001$), but there was no significant difference between the cumulative $CO_2$ loss from control (21.9 mg $CO_2$-C g $C^{-1}$) and treatments (17.5 mg $CO_2$-C g $C^{-1}$) by the final day of incubation.

After 49 days of incubation under wet-dry cycles, the Brady Soil from both the burial and the erosional transects emitted significantly more cumulative $CO_2$ (0.0183 g $CO_2$-C g $C^{-1}$) than Brady Soil incubated under continuously wet conditions (0.009 ± 0.0005 g $CO_2$-C g $C^{-1}$, $p < 0.001$). However, there was no significant difference between cumulative $CO_2$ loss in modern soils incubated under wet-dry cycles versus continuous wet conditions.

The order of magnitude of total $CO_2$ emission after 49 days followed the order erosional modern > erosional Brady > depositional modern > depositional Brady. Soils of the erosional transect (mean of 18.3 mg $CO_2$-C g $C^{-1}$) had significantly greater cumulative $CO_2$ loss compared to the depositional transect (mean of 16.7 ± 0.643 mg $CO_2$-C g $C^{-1}$, $p < 0.01$). Modern soil had significantly greater cumulative $CO_2$ loss (mean of 16.7 mg $CO_2$-C g $C^{-1}$) than Brady Soil (mean of 18.3 ± 0.390 mg $CO_2$-C g $C^{-1}$, $p < 0.001$), but the difference was not significant at the intermediate depth. Modern soil from the shallowest depth emitted significantly more cumulative $CO_2$ (19.2 mg $CO_2$-C g $C^{-1}$) than the deepest layer (13.9 mg $CO_2$-C g $C^{-1}$, $p < 0.05$). However, the opposite was observed in Brady Soil, where the deepest layer emitted more cumulative $CO_2$ (15.6 mg $CO_2$-C g $C^{-1}$) compared to the shallowest layer (20.4 mg $CO_2$-C g $C^{-1}$, $p < 0.05$). Among the control soils, although Brady Soil emitted more cumulative $CO_2$ than modern soil, there was no significant difference. This was likely due to large variation of the depth-pooled samples (in absence of control replicates), as a result of the much larger $CO_2$ loss from Brady Soil of the erosional transect at the greatest depth compared to other samples.

### 3.4 Decay rates and fraction sizes of soil organic matter pools

The decomposition rate of the slow pool and size of the fast pool under continuous wetting is shown in Fig. 4 and the decomposition rate of SOM (single pool) under wet-dry cycles is shown in Fig. 5. Statistical figures of merit of linear mixed-effects models are available online at DOI : doi: 10.17632/fjw646gpyf.1.

The slow-cycling SOM pool under continuous wetting decayed ca. 2000 times more slowly than the fast-cycling pool, with a significantly lower mean decay rate in the burial transect ($8.68 \cdot 10^{-6}$ $day^{-1}$ i.e., 315 years turnover time, henceforth referred to as TOT) compared to the erosional transect ($1.36 \cdot 10^{-5} \pm 6.82 \cdot 10^{-7}$ $day^{-1}$ i.e., 201 years TOT, $p < 0.01$). Thus, higher decay rates correspond to faster (shorter) turnover times throughout this section. The mean decay rate of the slow-cycling SOM pool of Brady Soil ($6.86 \cdot 10^{-6}$ $day^{-1}$ i.e., 399 years TOT) was significantly lower than that of modern soil ($1.54 \cdot 10^{-5}$ $day^{-1} \pm 6.82 \cdot 10^{-7}$, i.e., 178 years TOT, $p < 0.001$). The

mean decay rate of the slow-cycling SOM pool of modern soil in the burial transect was significantly greater at the greatest degree of burial ($1.53 \cdot 10^{-5}$ day$^{-1}$ i.e., 178 years TOT), compared to the lowest degree of burial ($9.97 \cdot 10^{-6}$ day$^{-1}$ i.e., 275 years TOT, $p < 0.05$).

The mean decay rate of the fast-cycling SOM pool of the erosional transect (0.130 day$^{-1}$ i.e., 7.68 days TOT) under continuous wetting was significantly higher (i.e., faster turnover) than that of the burial transect ($0.126 \pm 0.001$ day$^{-1}$ i.e., 7.96 days TOT, $p < 0.05$). The mean decay rate of the fast-cycling SOM pool of Brady Soil in the erosional transect was significantly greater at the greatest degree of erosion (0.144 day$^{-1}$ i.e., 6.96 days TOT) compared to the lowest degree of erosion (0.121 day$^{-1}$ i.e., 8.25 days TOT, $p < 0.01$).

The decay rate of SOM (one-pool model) under wet-dry cycles did not differ significantly among soils of different paleostatus or transect type. In the two-pool model, the decay rate of the slow-cycling SOM pool under wet-dry cycles was significantly higher in the erosional transect (0.007 day$^{-1}$ i.e., 129 days TOT) compared to the burial transect ($0.009 \pm .0002$ day$^{-1}$ i.e., 117 days TOT, $p < 0.05$), indicating faster SOM turnover where decay rates were higher. The decay rate of the fast-cycling SOM pool in the burial transect was significantly higher in modern soil ($8.11 \pm 1.94$ day$^{-1}$ i.e., 0.123 days TOT) compared to Brady soil (0.558 day$^{-1}$ i.e., 1.79 days TOT).

The slow-cycling pools of both modern and Brady Soil under continuous wetting contained a much greater proportion of total SOC ($> 96\%$) than the fast-cycling pool. The fraction size of the fast-cycling pool relative to the slow-cycling pool under continuous wetting was significantly greater in the erosional transect (0.014) compared to the burial transect ($0.012 \pm 0.0003$, $p < 0.01$) and significantly greater in modern soils (0.0173) compared to Brady Soil ($0.009 \pm 0.0003$, $p < 0.001$). The fraction size of the fast and slow pools tended to 0 and 1.0 respectively in all soils under wet-dry cycling, nullifying the statistical comparison results among soils of different paleostatus and transect types.

### 3.5 Decay rates and fraction sizes of soil organic matter pools in continuous wet versus wet-dry experiment

A summary of SOM decomposition model parameters (one-pool and two-pool) of the continuously wet and wet-dry cycling experiments is shown in Table 2. Statistical figures of merit of linear mixed-effects models are available online at DOI : doi: 10.17632/fjw646gpyf.1.

With the one-pool models, the continuously wet soils had a significantly higher decay rate (0.00865 day$^{-1}$ i.e., 116 days TOT) compared to the wet-dry cycles (0.00714 day$^{-1}$ i.e., 140 days TOT, $p < 0.01$), indicating faster turnover under continuous wetting. In the burial transect, the one-pool decay constant of the continuous wet experiment was significantly higher (0.0103 day$^{-1}$ i.e., 97.4 days TOT) than that of the wet-dry cycling experiment (0.00690 day$^{-1}$ i.e., 145 days TOT, $p < 0.001$). However, there was no significant difference between the decay constant of the continuous wet and wet-dry experiments in erosional transects. These trends were observed in both Brady and modern soils.

Among the control soils with one-pool models, the continuous wet experiment had a significantly higher decay rate (0.0376 $day^{-1}$ i.e., 26.6 days TOT) compared to the wet-dry cycling experiment (0.00146 $day^{-1}$ i.e., 179 days TOT, $p < 0.001$), again meaning faster decomposition under continuous wetting. This was true in both burial (continuous wet k = 0.0374 $day^{-1}$ i.e., 26.7 days TOT and wet-dry k = 0.00372 i.e., 268 days TOT) and erosional (k = 0.0377 $day^{-1}$ i.e., 26.5 days TOT and wet-dry k = 0.00746 $day^{-1}$ i.e., 134 days TOT) transects, as well as Brady (continuous wet k = 0.0376 $day^{-1}$ i.e., 26.6 days TOT and wet-dry k = 0.00871 $day^{-1}$ i.e., 115 days TOT) and modern (continuous wet k = 0.0375 $day^{-1}$ i.e., 26.7 days TOT and wet-dry k = 0.00248 $day^{-1}$ i.e., 404 days TOT) soils.

With the two-pool models, the decay rate of the slow-cycling SOM pool in the continuously wet experiment was significantly lower ($1.11 \cdot 10^{-5}$ $day^{-1}$ i.e., 246 years TOT) than that of the wet-dry cycling experiment (0.00812 $day^{-1}$ i.e., 123 days TOT, $p < 0.001$), reflecting faster turnover in the wet-dry treatments. This was true in both Brady (continuously wet k = $6.86 \cdot 10^{-6}$ $day^{-1}$ i.e., 399 years TOT, wet-dry k = 0.0083 $day^{-1}$ i.e., 120 days TOT) and modern (continuously wet k = $1.54 \cdot 10^{-5}$ $day^{-1}$ i.e., 178 years TOT, wet-dry k = 0.00793 $day^{-1}$ i.e., 126 days TOT) soils, as well as both burial (continuously wet k = $8.68 \cdot 10^{-6}$ $day^{-1}$ i.e., 316 years TOT, wet-dry k = 0.00773 $day^{-1}$ i.e., 129 days TOT) and erosional (continuously wet k = $1.36 \cdot 10^{-5}$ $day^{-1}$ i.e., 202 years TOT, wet-dry k = 0.0085 $day^{-1}$ i.e., 118 days TOT) transects, and in all depth layers.

The decay rate of the fast-cycling SOM pool in modern soil was significantly higher in the wet-dry cycling experiment (8.11 $day^{-1}$ i.e., 0.123 days TOT) compared to the continuously wet experiment (0.127 $day^{-1}$ i.e., 7.89 days TOT, $p < 0.001$), indicating a much faster turnover response to rewetting. The decay rate of the fast-cycling pool in the erosional transect was also significantly higher in the wet-dry cycling experiment (5.148 $day^{-1}$ i.e., 0.194 days TOT) compared to the continuously wet experiment (0.130 $day^{-1}$ i.e., 7.68 days TOT). Separating these effects by depth revealed that the significance of the difference between the fast pool decay rate in modern soils was more evident at the intermediate and greatest depth. The decay rate of the fast-cycling SOM pool did not differ significantly between continuously wet and wet-dry cycling experiments in Brady soils or in the burial transect.

Among the control soils with two-pool models, the continuous wet experiment had significantly lower slow pool decay rate ($1 \cdot 10^{-8}$ $day^{-1}$ i.e., 274 000 years TOT) compared to the wet-dry cycling experiment (k = 0.005 $day^{-1}$ i.e., 200 days TOT, $p < 0.01$), again corresponding to much faster turnover in the wet-dry treatments. This was true in both the burial and erosional transects, modern and Brady Soil and at all depths.

The decay rate of the fast-cycling SOM pool of control Brady Soil was significantly higher in the wet-dry cycling experiment (0.0556 $day^{-1}$ i.e., 18.0 days TOT) compared to the continuously wet experiment (10.3 $day^{-1}$ i.e., 0.0971 days TOT). This was true in both burial and erosional transects. In modern soils, however, there was no significant difference between decay rates of fast-cycling SOM in continuously wet versus wet-dry cycling experiments.

The fraction size of the slow-cycling SOM pool in the wet-dry cycling experiment was significantly larger (0.999) than that of the continuously wet experiment (0.987, $p < 0.001$) - this was true for both Brady and modern soils, across erosional and burial transects and at all depths. It follows that the fraction size of the fast-cycling SOM pool in wet-dry cycling experiments was significantly smaller (0.001) than that of the continuously wet experiment (0.0131, $p < 0.001$) for soils of all transect types, paleostatus groups and depth categories. There was no significantly difference between fraction sizes of the slow-cycling SOM pool among the controls of the wet-dry cycling and continuously wet experiment; the fast-cycling pool was also similar among control soils of the two experiments.

### 3.6 Relationships between soil properties and carbon dynamics

The true versus predicted values MLR models for prediction of decomposition rates of the fast- and slow-cycling pools as well as the fraction size of the slow pool are shown in the Appendix, Fig. A2. A matrix showing the correlation between these variables is given in Fig. 6. The intercept, coefficients of explanatory variables, RMSE and $R^2$ of the best-performing MLR models, are summarized in Table 3 and the full equations are in the Appendix (Multiple linear regression equations).

The MLR models for prediction of decay rates of SOM under continuous wetting had better model fit ($R^2 > 0.80$) compared to those for predictions of SOM pool fraction size ($R^2 = 0.44$). From the MLR equations, we deduce that soil properties with the greatest coefficients had the most important effects on the SOM decay rate and fraction size model parameters. While SAR increased the rate of decay and decreased the size of the of the slow pool, an opposite trend is observed in the fast pool.

TOC and pH also increased the decay rate of the fast-cycling SOM pool under continuous wetting, while the slow pool decay rate decreased with increasing TIC. TOC and TIC increased the fraction size of the slow pool at the expense of fraction size of the fast pool. When considering effects of these factors individually, SAR, TOC, TIC and pH did not have significant correlation with SOM decomposition parameters (Fig. 6). However, exchangeable Mg and K content were significantly correlated with the decay rate of the fast (negative correlation) and slow (positive correlation) pools (Fig. 6).

The true versus predicted values MLR models for prediction of the decomposition rate of SOM (one-pool system) under wet-dry cycles are shown in the Appendix, Fig A3. A matrix showing the correlation between these variables is given in Appendix, Fig. A4.

The intercept, coefficients of explanatory variables, RMSE and $R^2$ of the best-performing MLR model for prediction of the decay rate, are given summarized in Table 3 and the full equation is in the Appendix (Multiple linear regression equations).

SAR decreased the decay rate of SOM under wet-dry cycles. Clay and TOC content increased the decay rate of SOM. Exchangeable Ca, Mg content decreased the decay rates of both pools. Considering these parameters individually (correlation coefficients) revealed a weak correlation with k. Therefore MLR, where k is modeled as a function of all predictors together, demonstrates that the combination of these variables explained most variance, while no single predictor explained much variance on its own.

# 4 Discussion

## 4.1 Stabilization of soil organic matter by burial

While our study characterizes decomposition dynamics using respirometry and radiocarbon-based modeling, we did not directly measure the molecular mechanisms responsible for differential SOC stability. Specifically, we did not quantify the chemical composition of mineral-associated organic matter, the nature of organo–mineral bonds, or microbial community composition. As a result, the mechanistic interpretations presented here are necessarily indirect.

The interpretations proposed in this study build on prior molecular and fractionation-based analyses conducted on the same soils and geomorphic transects (Marin-Spiotta et al. 2014; Dolui et al. 2026). That work documented enhanced mineral association and cation-mediated stabilization in buried profiles. Rather than repeating those analyses, the present study extends this framework by quantifying how these stabilization contexts translate into differences in SOC turnover rates and pool structure under contrasting moisture regimes.

Brady Soil subjected to continuous wetting exhibited lower cumulative $CO_2$ evolution than modern soils across both erosional and depositional transects (Fig. 2; Appendix Fig. 3). This pattern indicates reduced microbial mineralization in buried paleosols relative to surface soils under sustained moisture availability.

Multiple mechanisms may contribute to this enhanced stability, although their relative importance cannot be resolved with the current dataset. Previous work at this site reported elevated exchangeable $Ca^{2+}$ concentrations in Brady soils and linked Ca-mediated flocculation to increased aggregate stability (Dolui et al., in press). Our results are consistent with this interpretation. Specifically, Ca concentration was a positive predictor of slow-pool size in the MLR model. However, we did not directly measure aggregation or flocculation processes. As a result, the pathway linking Ca availability to reduced decomposition remains uncertain. Reduced decay could arise from physical protection within aggregates, reduced microbial access to substrates, or changes in solute diffusivity. Within the scope of this study, $Ca^{2+}$ therefore emerges as a statistically robust predictor of SOC pool structure, rather than a resolved mechanistic driver.

The potential contribution of pyrogenic carbon to SOC persistence in Brady soils is supported by prior molecular analyses from this site. These analyses identified condensed aromatic compounds consistent with fire-derived inputs (Marin-Spiotta et al. 2014). Pyrogenic carbon was not quantified in the present study, and its direct influence on decomposition rates cannot be evaluated here. Nonetheless, its documented persistence provides important context for interpreting the slow-cycling SOC pool observed in Brady soils. Our results are therefore compatible with a stabilization legacy established during Brady Soil formation, rather than evidence of an active pyrogenic control on contemporary decomposition.

Modern soils exhibited a slightly larger relative size of the fast-cycling SOM pool than Brady soils, which likely reflects recent organic inputs. Direct comparison of decay parameters further highlights differences in SOM persistence between soil types (Fig. 4). The slow-cycling pool in Brady soils from the most erosional transect had

significantly lower decay rates under continuous wetting than the corresponding pool in modern soils. This provides clear evidence of greater SOM persistence in the paleosol.

Across all treatments, the slow pool decayed approximately 2000 times more slowly than the fast pool. Brady soils exhibited turnover times (TOTs) of approximately 399 years, whereas modern soils exhibited TOTs of approximately 178 years. The MLR models further showed a negative relationship between slow-pool decay rate ($k_{slow}$) and both total inorganic carbon (TIC) and exchangeable $Mg^{2+}$ (Equation A1). Although $CaCO_3$ cementation was not pronounced, positive correlations between TOC, TIC, and Ca in Brady soils from erosional transects (Dolui et al., in press) suggest that carbonate-associated phases may contribute to stabilization where shallow wetting promotes near-surface carbonate precipitation.

The association between finer texture and reduced SOC decomposition observed in this study aligns with established theory linking clay-rich soils to enhanced mineral-associated organic matter formation (Six et al. 2002). Clay content was a significant predictor of slow-pool dynamics in the MLR models, indicating that particle size exerts a first-order control on SOC accessibility. However, because mineral surface chemistry and sorption energetics were not resolved, texture is interpreted here as a proxy for stabilization potential rather than as a direct mechanistic control.

The slow-cycling SOM pool dominated total soil C, accounting for more than 96% of SOC (Fig. 4b). The size of this pool increased with increasing TOC and TIC (Equation A1) and was accompanied by a corresponding decline in the fast-cycling pool. The fast pool consistently represented a larger fraction of total SOC in modern soils than in Brady soils, and in erosional transects than in burial transects. Together, these patterns indicate stronger stabilization in buried paleosols and underscore the central role of the slow-cycling pool in long-term SOC persistence.

Apparent relationships between sodium adsorption ratio (SAR), exchangeable cations, decay rates, and pool sizes in the MLR models (Equations A1, A2, A3, and A4; Fig. 6) should be interpreted cautiously. These correlations may reflect shared depth-dependent trends rather than direct mechanistic links. Both TOC and microbial biomass typically decline with depth (Fierer and Schimel 2003; Xiang et al. 2008), which contributes to reduced respiration in deeper Brady soils. At the same time, Na tends to accumulate at depth through leaching (Dolui et al., in press), with accumulation depth depending on precipitation and soil water status.

## 4.2 Destabilization of SOM by erosion and moisture variability

Greater cumulative C loss from shallower soils, combined with a smaller fast-cycling SOM pool and a significantly higher slow-pool decay rate in erosional Brady soils compared to depositional Brady soils (Fig. 4a), highlights the destabilizing effect of surface exposure. This pattern indicates that erosion weakens burial-associated protection.

$CO_2$ pulses during the initial phase of wet–dry cycling were larger in erosional transects than in burial transects (Fig. A1). These pulses suggest enhanced mineralization in Brady soils closer to the surface. One likely explanation is priming by root exudates and fresh organic inputs, amplified by bioturbation (Pausch et al. 2016; McMurtry

et al. 2024). This interpretation is supported by higher fraction modern values in erosional Brady soils relative to depositional Brady soils, as well as by convergence of slow-pool fraction modern values toward those of modern soils (Dolui et al. 2026).

Enhanced decomposition in shallower Brady soils likely reflects both legacy exposure and contemporary environmental conditions. Shallower positions experience more frequent wetting and greater oxygen diffusion, which can prime microbial communities for rapid response following rewetting. Separating long-term exposure effects from ongoing environmental controls would require experimental manipulation of burial depth, which represents an important avenue for future research.

In the wet–dry experiment, erosion effects were further expressed in decay dynamics. Slow pools decayed faster in erosional transects than in burial transects, whereas fast pools decomposed more rapidly in modern soils than in Brady soils. The fraction of the slow pool was smaller under continuous wetting than under wet–dry cycling, indicating greater allocation to slow-cycling carbon under variable moisture. However, the slow pool also exhibited substantially higher decay rates under wet–dry cycling. This suggests that apparent stabilization under variable moisture is transient and may be offset over time by depletion of passive C reserves.

The accelerated decay of slow-pool SOC under drying–rewetting cycles demonstrates that burial-associated protection is not absolute, even for millennially persistent carbon. Potential mechanisms include aggregate disruption, increased solute transport, or shifts in microbial accessibility. While the present study cannot resolve these pathways, it clearly documents the outcome: enhanced decomposition of previously slow-cycling SOC under moisture variability.

Moisture variability also amplified turnover of the fast-cycling pool. Decay rates of the fast pool increased under wet–dry cycling, particularly in modern soils and erosional transects. This pattern supports the interpretation that fresh organic inputs and surface exposure accelerate labile C turnover under fluctuating moisture. The MLR model reinforces this interpretation by revealing a positive relationship between TOC and fast-pool decay rate (Equation A4). In contrast, the absence of strong moisture effects in Brady soils suggests that burial dampens moisture-driven variability in labile C decomposition.

McDowell et al. (2022) simulated soil hydrology for the Brady Soil, overlying loess, and modern soil using measured hydraulic properties and regional weather data from 2009–2019. Modeled water contents remained low and relatively constant below 1.5 m depth, including within the Brady Soil, with only rare deep wetting events following major rainfall. Paleoclimate reconstructions indicate that the depth of frequent wetting would have been even shallower during drier-than-modern periods over the past 10,000 years (Miao et al. 2007). Together, these results suggest that prolonged dry conditions played a major role in OC sequestration where the Brady Soil is deeply buried, whereas erosion and increased moisture variability could promote renewed C loss.

Geomorphic position integrates multiple stabilization controls by regulating burial depth, moisture exposure, oxygen availability, and the persistence of mineral–organic associations. In this sense, geomorphic context operates as a higher-order constraint that modulates how chemical and physical stabilization mechanisms are expressed

through time. These findings challenge the common assumption in soil carbon modeling that geomorphic context can be neglected when parameterizing decomposition rates. Our results show that erosional exposure accelerates slow-pool decay under continuous wetting, and that wet–dry cycling destabilizes slow-pool carbon regardless of landscape position. For Earth system models that treat subsoil carbon as a passive reservoir, these dynamics represent a substantial and underappreciated vulnerability. Accurately predicting SOC responses to changing precipitation regimes therefore requires explicit consideration of burial depth and exposure history, which are rarely incorporated into current modeling frameworks.

# 5 Conclusion

When interpreted alongside prior molecular- and fractionation-based analyses from this site (Marin-Spiotta et al., 2014; Dolui et al., in press), our results suggest that long-term SOC persistence in Brady soils arises from the convergence of mineral association, cation-mediated stabilization, and limited environmental exposure. The present study extends this framework by demonstrating that these stabilization contexts remain vulnerable to hydrologic perturbation and geomorphic re-exposure. Although this study does not resolve molecular-scale mechanisms directly, it demonstrates that decomposition parameters derived from incubation and radiocarbon modeling are highly sensitive to landscape history – an effect that must be accounted for even when detailed chemical data are unavailable.

Our study demonstrates that SOC decomposition is strongly shaped by soil moisture regime and landscape position, with modern and Brady soils responding differently to continuous wetting versus drying–rewetting cycles. Water availability exerted disproportionate effects in erosional settings where surface exposure enhanced substrate diffusivity, highlighting the destabilizing role of re-exposure and moisture fluctuations.

Drying–rewetting cycles led to greater C losses from Brady soils than continuous wetting, despite modeling results indicating dominance of the slow pool and depletion of labile C. This treatment also accelerated fast pool decay in modern soils and erosional transects, while burial dampened such variability in Brady soils. Fraction sizes shifted accordingly: wet–dry cycles increased the proportion of the slow pool and reduced the fast pool fraction, suggesting redistribution of SOC toward more stabilized forms under fluctuating moisture.

Depth further constrained SOM persistence, with slow pool decay constants declining in deeper Brady soils from depositional transects. Faster turnover in shallow layers reflects greater microbial accessibility and responsiveness to surface-driven processes, underscoring the importance of geomorphic context - transect type, burial depth, and soil structure - over intrinsic SOM chemistry.

Comparisons across models showed that continuous wetting accelerated overall decay, particularly in burial transects, while wet–dry cycles disproportionately destabilized the slow pool that dominates SOC. This dual effect - rapid labile C turnover under moisture fluctuations coupled with erosion of long-lived SOM persistence - points to heightened vulnerability of buried carbon under future precipitation variability.

Overall, the fate of ancient soil carbon under climate change will depend on both its burial history and prevailing moisture regime. Integrating these contrasting controls on fast- and slow-cycling pools into Earth system models is essential for improving predictions of soil carbon vulnerability and climate feedback.

**Funding.** This work was supported by the National Science Foundation (EAR awards 1623814, 1623810, and 1623812), the University of California, Merced, and the Ted and Jan Falasco Endowment.

**Competing interests.** The authors have no relevant financial or non-financial interests to disclose.

**Data availability.** Full dataset for soil incubation and statistical analyses are available at DOI: doi: 10.17632/fjw646gpyf.1.

**Author contributions.** All authors contributed to the study conception and design. Material preparation, data collection, and analysis were performed by Manisha Dolui, Teneille Nel, Abbygail R. McMurtry, Stephanie Chacon, Laura M. Phillips, Teamrat Ghezzehei, Joseph A. Mason, Erika Marin-Spiotta, Marie-Anne de Graaff and Asmeret Asefaw Berhe. The first draft of the manuscript was written by Manisha Dolui and Teneille Nel. All authors commented on previous versions of the manuscript and approved the final manuscript.

**Acknowledgments.** We acknowledge financial support for this work from the National Science Foundation (EAR awards 1623814, 1623810, and 1623812) and the Ted and Jan Falasco Endowment, fellowships and grants awarded by the Graduate Division at the University of California, Merced (UCM), and the UCM Environmental Systems Graduate Group. We are grateful to Dr. Sora Kim and Dr. Robin Trayler for their support at the UCM Stable Isotope Lab. We also thank R. and D. Whiting for providing access to the Wauneta, Nebraska, field sites. ChatGPT was used for language editing and sentence refinement and the authors take full responsibility for the output.

**Tables and figures.**

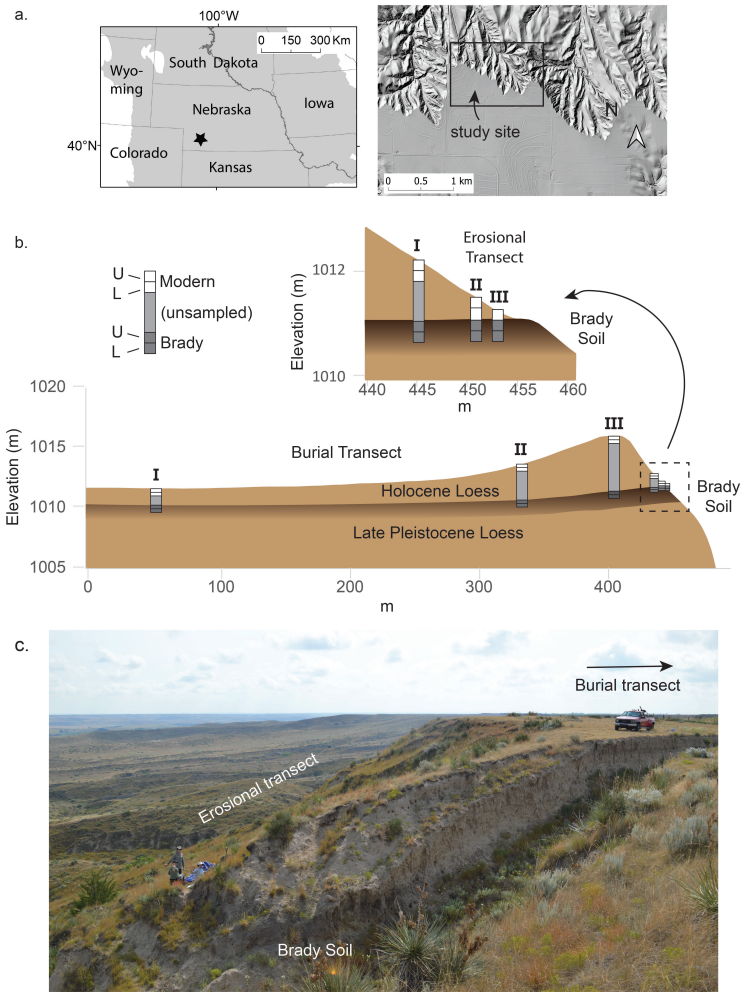


**Fig. 1** Study site location, stratigraphy, and sampling scheme. a. Location of the study site within the Great Plains ecoregion (grayshade) and shaded relief map illustrating topographic setting of study site. b. Vertical cross-sections illustrating the sampling scheme relative to modern land surface topography, the Brady Soil, and loess above and below it at study site. Weakly developed horizons of modern soil and paleosols within the Holocene loess (Miao et al., 2007) not shown. Details based on one pair of burial and erosional transects but representative of all three. c. Photo illustrating topography and native grassland vegetation at one pair of transects. Truck is near deepest profile (III) on burial transect; other burial transect points are not visible. Brady Soil is exposed in an old roadcut in foreground; erosional transect is located on intact slope beyond roadcut. Figure adapted from Dolui et al. (2026)

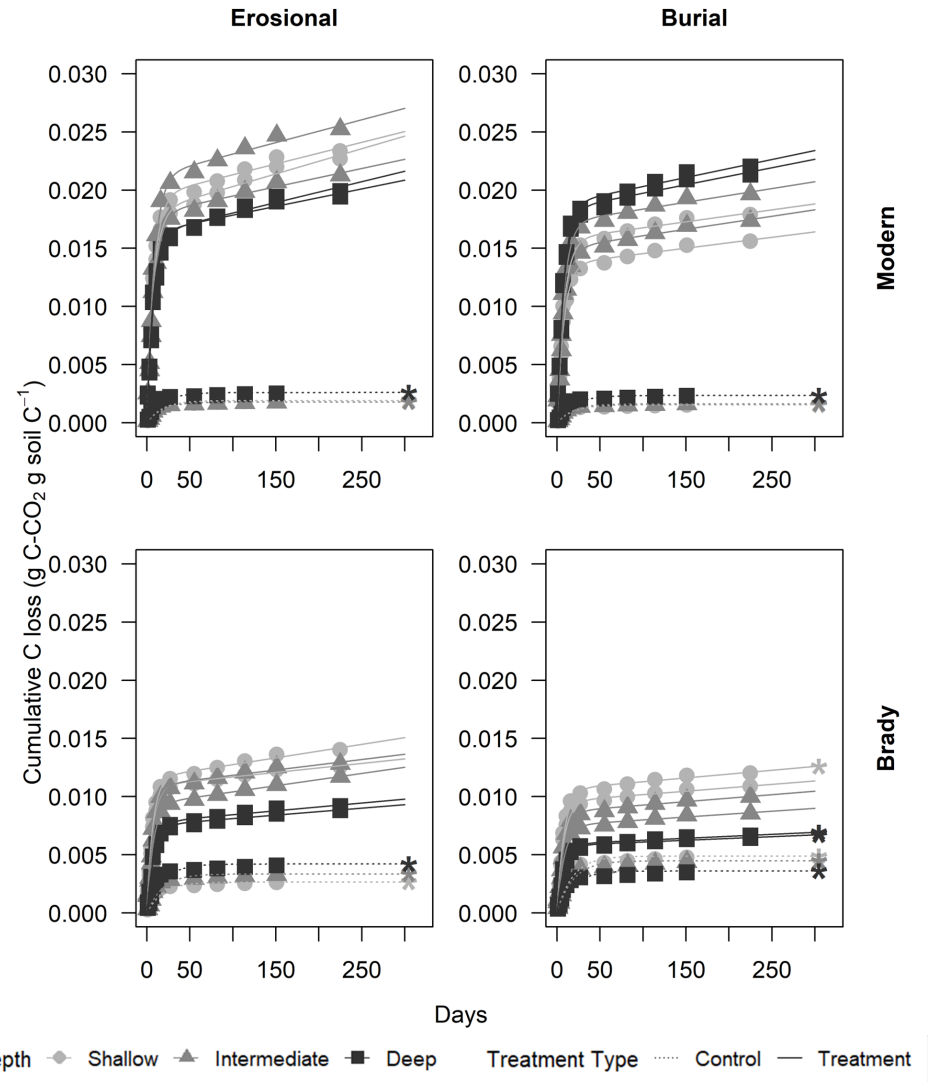


**Fig. 2** Cumulative respiratory $CO_2$ from modern and Brady Soil sampled from three depths representing varying degrees of burial/erosional exposure (two technical replicates each). Soils were maintained at a constant moisture content of 60% water holding capacity (WHC). Lines depict a two-pool first-order decay model, fitted using a non-linear least-squares function. The dotted line represents the control (5% WHC).

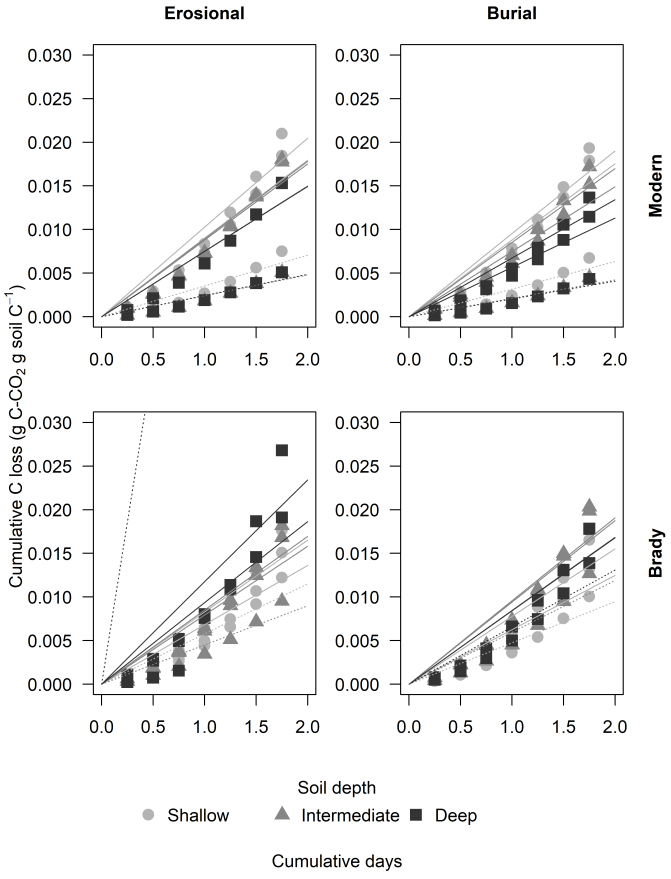


**Fig. 3** Cumulative respiratory $CO_2$ flux from modern and Brady Soil sampled from three depths representing varying degrees of burial/erosional exposure (two technical replicates each). Soils were wetted to a moisture content of 60% water holding capacity (WHC) and allowed to dry to 5% WHC. Lines depict a one-pool first-order decay model, fitted using a non-linear least-squares funtcion. The dotted line represents the control (constant 5% WHC); one control Brady soil sample of the erosional transect had an outlier point not shown due to scale. Asterisks (*) indicate control samples maintained at 5% WHC

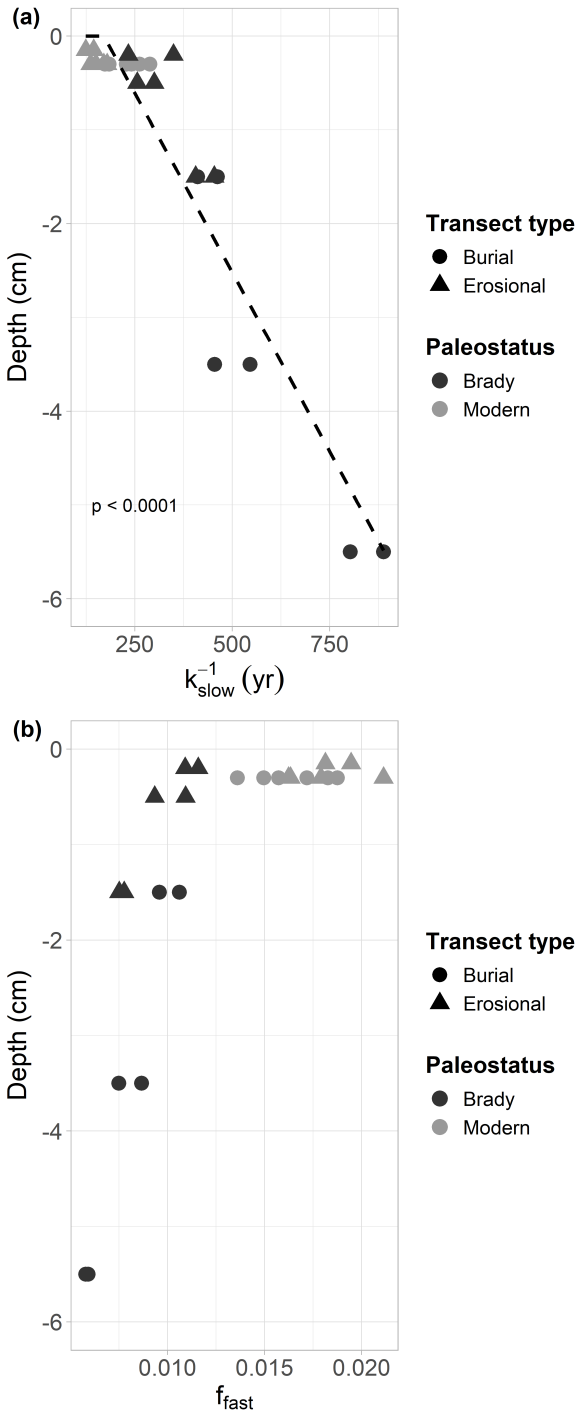


**Fig. 4** Decay constant of the slow cycling pool of modern and Brady soils incubated under continuously wet conditions. Samples collected from depositional and erosional transect types. Dotted line indicates exponential decay. Figure b indicates the size of the fast-cycling pool at different depths of the modern and Brady soils in depositional and erosional transect types.

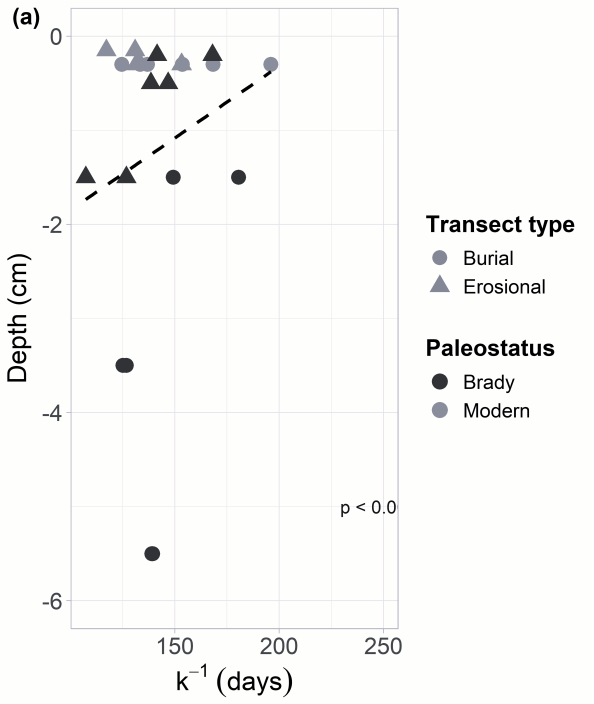


**Fig. 5** Decay constant of modern and Brady soil organic matter incubated under wet-dry cycling conditions. Samples collected from depositional and erosional transect types. Dotted line indicates exponential decay.

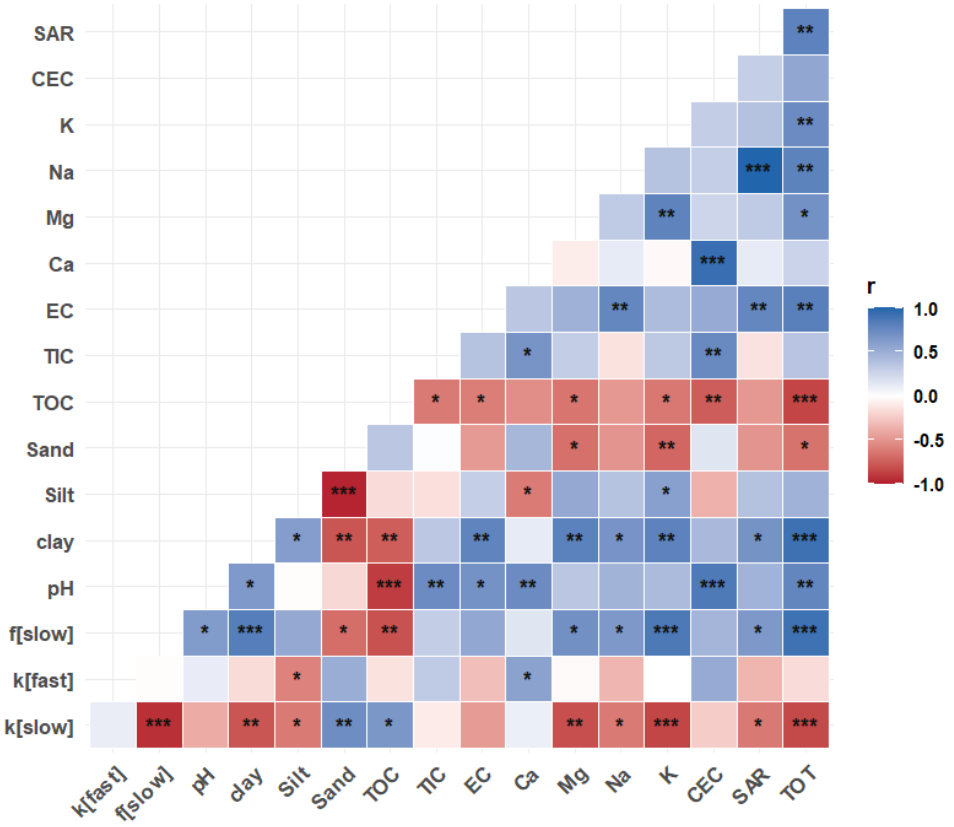


**Fig. 6** Correlation between soil physicochemical properties and modeled soil organic matter decomposition parameters (decay constant, k, and fraction of C in slow pool, f) for fast- and slow-cycling pools in modern and Brady soils incubated under continuously wet conditions. Decomposition parameters were obtained by multiple linear regression across burial and erosional transects. The statistical significance of each correlation is denoted by asterisks (*** for $p<0.001$, ** for $p<0.01$, * for $p<0.05$).

**Table 1** General physicochemical (mean +- standard deviation) of soils used in the incubation experiment, grouped by transect type and paleostatus

| **Transect type** | Burial | | Erosional | |
|---|---|---|---|---|
| **Paleostatus** | Brady | Modern | Brady | Modern |
| pH | 7.77 ± 0.04 | 6.89 ± 0.32 | 7.68 ± 0.12 | 7.41 ± 0.10 |
| Clay (%) | 9.48 ± 0.75 | 6.13 ± 0.64 | 7.62 ± 0.44 | 6.29 ± 0.48 |
| Silt (%) | 59.31 ± 0.44 | 56.24 ± 5.76 | 55.73 ± 4.88 | 53.67 ± 1.51 |
| Sand (%) | 31.24 ± 0.94 | 37.62 ± 6.39 | 36.64 ± 5.22 | 40.08 ± 1.92 |
| TOC content | 0.45 ± 0.06 | 1.03 ± 0.20 | 0.56 ± 0.10 | 0.93 ± 0.17 |
| TIC content | 0.24 ± 0.11 | 0.09 ± 0.03 | 0.28 ± 0.04 | 0.25 ± 0.03 |
| EC (dS $m^{-1}$) | 5.41 ± 0.32 | 2.26 ± 0.43 | 3.05 ± 0.47 | 3.57 ± 0.35 |
| CEC (cmolc $kg^{-1}$) | 22.86 ± 0.54 | 15.17 ± 3.54 | 23.31 ± 3.52 | 20.59 ± 1.83 |
| Turnover time (y) | 15654 ± 2440 | 576.4 ± 126 | 8327 ± 2732 | 1451 ± 673 |
| CN ratio | 10.00 ± 0.45 | 9.24 ± 0.21 | 10.96 ± 0.20 | 9.76 ± 0.25 |

**Table 2** Soil organic matter (SOM) decomposition parameters (decay rate $k$ of one-pool model, decay rates of fast- ($k_{\text{fast}}$) and slow-cycling ($k_{\text{slow}}$) SOM pools, and fraction sizes of fast ($f_{\text{fast}}$) and slow ($f_{\text{slow}}$) pools, grouped by experiment, transect type, and paleostatus.

| **Experiment** | CW | | | | WD | | | |
|---|---|---|---|---|---|---|---|---|
| **Transect type** | Burial | | Erosional | | Burial | | Erosional | |
| **Paleostatus** | Brady | Modern | Brady | Modern | Brady | Modern | Brady | Modern |
| $k$ (one pool) | 0.0107 | 0.0099 | 0.0069 | 0.0072 | 0.0071 | 0.0067 | 0.0074 | 0.0074 |
| $k_{\text{slow}}$ | <0.0001 | <0.0001 | <0.0001 | <0.0001 | 0.0080 | 0.0074 | 0.0086 | 0.0084 |
| $k_{\text{fast}}$ | 0.1250 | 0.1264 | 0.1333 | 0.1270 | 0.6931 | 6.3419 | 0.4222 | 9.8728 |
| $f_{\text{slow}}$ | 0.9920 | 0.9836 | 0.9903 | 0.9818 | 0.9990 | 0.9990 | 0.9990 | 0.9990 |
| $f_{\text{fast}}$ | 0.0080 | 0.0164 | 0.0097 | 0.0182 | 0.0010 | 0.0010 | 0.0010 | 0.0010 |

**Table 3** Summary of multiple linear regression models showing key positive (+) and negative (-) predictors of model parameters (proportions of fast and slow cycling fractions of TOC, i.e., $f_f$ and $f_s$ and the corresponding decay rate constants $k_f$ and $k_s$), model performance ($R^2$), and root mean square error (RMSE).

| Model parameter | Key (+) predictors | Key (-) predictors | $R^2$ | RMSE |
|---|---|---|---|---|
| $k_{\text{slow}}$ | clay, Ca, EC | SAR, Mg, K, pH, TOC, TIC | 0.98 | $7.01 \times 10^{-7}$ |
| $k_{\text{fast}}$ | SAR, clay, Ca, Mg, TIC | K, EC, pH | 0.95 | $1.41 \times 10^{-3}$ |
| $f_{\text{slow}}$ | SAR, Mg, K, pH, TIC | clay, Ca, EC, TOC | 0.97 | $8.38 \times 10^{-4}$ |
| $f_{\text{fast}}$ | clay, Ca, EC, TOC | SAR, Mg, K, pH, TIC | 0.97 | $8.38 \times 10^{-4}$ |
| $k_{\text{one-pool}}$ | clay, K, pH, TOC | SAR, Ca, Mg | 0.94 | $2.15 \times 10^{-4}$ |

# Appendix A

**Table A1** Sampling depth intervals (standard deviation in brackets for n = 3) of modern (surface) and Brady (burial) soils along two types of transects, where degrees of burial or exposure increase from degrees I to III. Table adapted from Dolui et al., in press.

| | | **Transect Type** | | | | | |
|---|---|---|---|---|---|---|---|
| | | Erosional | | | Burial | | |
| | | **Degree** | | | | | |
| | Depth (cm) | III | II | I | I | II | III |
| **Paleostatus** | Modern | 0-19 (2.5) | 0-19 (3.2) | 0-18 (3.5) | 0-30 (0.6) | 0-29 (0.6) | 0-29 (0.0) |
| | | NA | 19-38 (3.6) | 18-36 (3.5) | 30-60 (0.6) | 29-59 (2.3) | 29-59 (2.3) |
| | Brady | 20-50 (1.2) | 50-80 (0.0) | 150-180 (0.0) | 100-130 (4.0) | 300-330 (9.3) | 550-580 (6.7) |
| | | 50-80 (0.4) | 80-120 (0.0) | 180-210 (2.9) | 130-160 (4.5) | 330-360 (2.6) | 580-610 (5.6) |

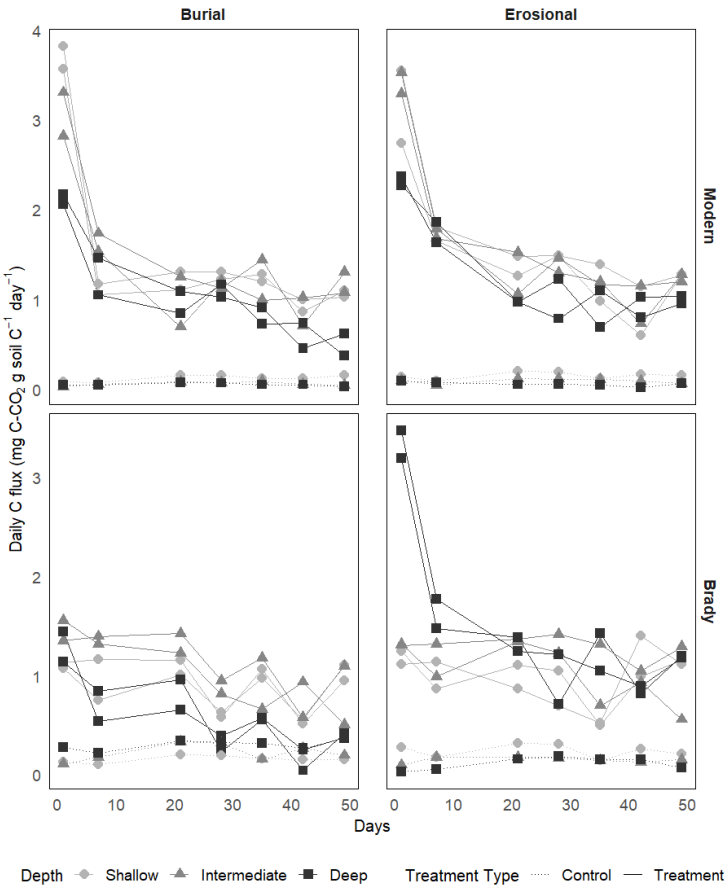


**Fig. A1** Daily respiratory $CO_2$ flux from modern and Brady Soil sampled from three depths representing varying degrees of burial/erosional exposure (two technical replicates each). Soils were wetted to a moisture content of 60% water holding capacity (WHC) and allowed to dry to 5% WHC. The dotted line represents the control (constant 5% WHC).

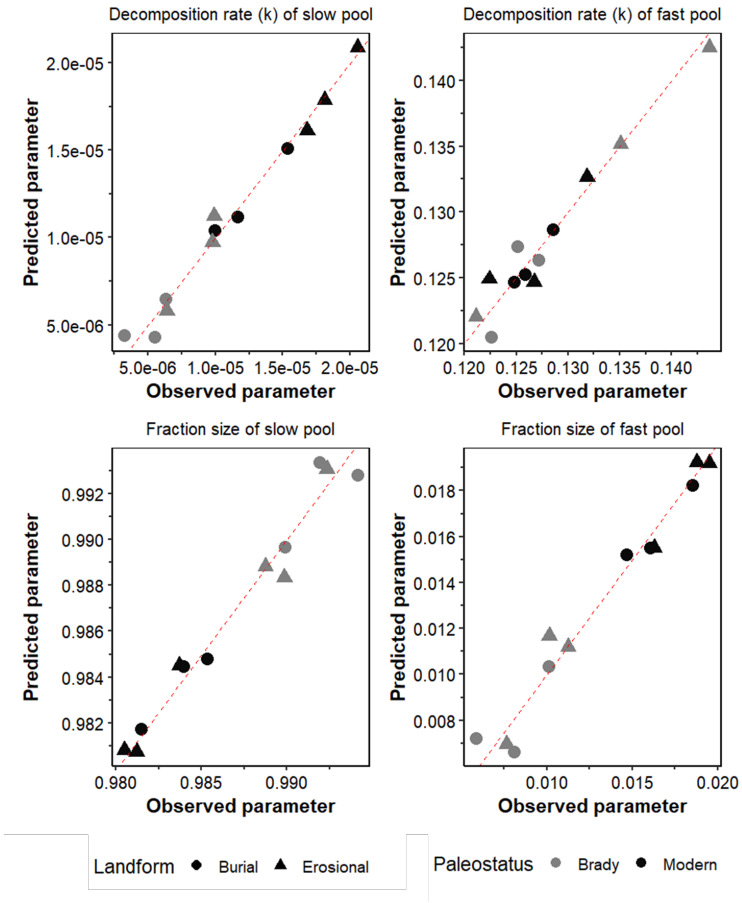


**Fig. A2** True versus predicted soil organic matter decomposition parameters (decay constant, k, and fraction of C in slow pool, f) for fast- and slow-cycling pools in modern and Brady soils incubated under continuously wet conditions. These parameters were obtained by multiple linear regression across burial and erosional transects. Red dotted line represents y = x.

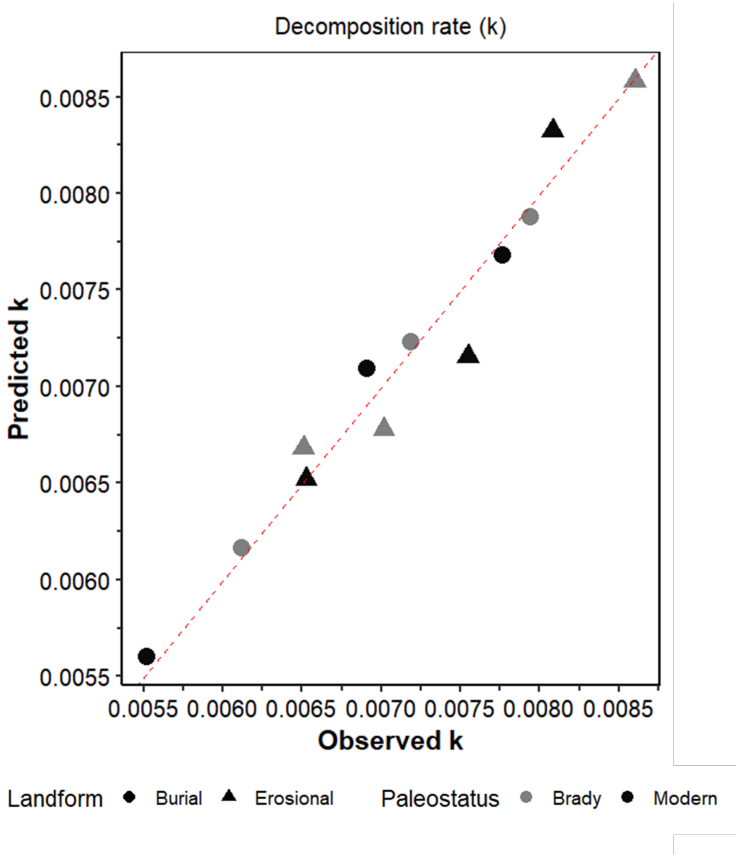


**Fig. A3** True versus predicted soil organic matter decay constant, k) in modern and Brady soils incubated under wet-dry cycling conditions. These parameters were obtained by multiple linear regression across burial and erosional transects. Red dotted line represents y = x.

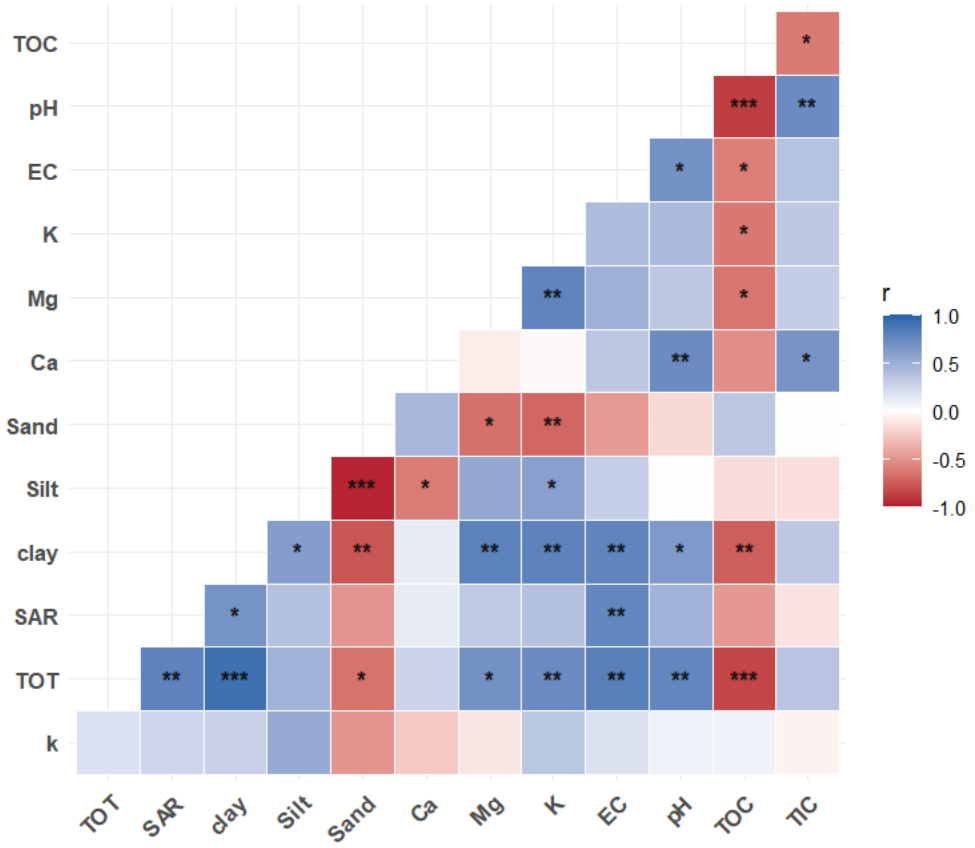


**Fig. A4** Correlation between soil physicochemical properties and modeled soil organic matter decomposition parameters (decay constant, k, and fraction of C in slow pool, f) for fast- and slow-cycling pools in modern and Brady soils incubated under wet-dry cycles. Decomposition parameters were obtained by multiple linear regression across burial and erosional transects. The statistical significance of each correlation is denoted by asterisks (*** for $p<0.001$, ** for $p<0.01$, * for $p<0.05$).

## A.1 Multiple linear regression equations

$$k_{slow} = 0.0000532 - 0.0000979 \cdot SAR + 0.00000225 \cdot clay + 0.000000395 \cdot Ca - 0.00000622 \cdot Mg - 0.00000271 \cdot K + 0.00000347 \cdot EC - 0.00000618 \cdot pH - 0.00000687 \cdot TOC - 0.0000275 \cdot TIC \quad (A1)$$
$$RMSE : 0.000000701, \quad R^2 : 0.98$$

$$k_{fast} = 0.215 + 0.0189 \cdot SAR + 0.00344 \cdot clay + 0.0026 \cdot Ca + 0.00204 \cdot Mg - 0.000302 \cdot K - 0.00513 \cdot EC - 0.0196 \cdot pH + 0.0146 \cdot TIC \quad (A2)$$
$$RMSE : 0.00141, \quad R^2 : 0.95$$

$$f_{slow} = 0.976 + 0.0732 \cdot SAR - 0.000362 \cdot clay - 0.000241 \cdot Ca + 0.00138 \cdot Mg + 0.00283 \cdot K - 0.00288 \cdot EC + 0.00174 \cdot pH - 0.000707 \cdot TOC + 0.0298 \cdot TIC \quad (A3)$$
$$RMSE : 0.000838, \quad R^2 : 0.97$$

$$f_{fast} = 0.0243 - 0.0732 \cdot SAR + 0.000362 \cdot clay + 0.000241 \cdot Ca - 0.00138 \cdot Mg - 0.00283 \cdot K + 0.00288 \cdot EC - 0.00174 \cdot pH + 0.000707 \cdot TOC - 0.0298 \cdot TIC \quad (A4)$$
$$RMSE : 0.000838, \quad R^2 : 0.97$$

$$k(one - pool) = -0.00641 - 0.00308 \cdot SAR + 0.000599 \cdot clay - 0.000141 \cdot Ca - 0.0015 \cdot Mg + 0.00118 \cdot K + 0.00159 \cdot pH + 0.002 \cdot TOC \quad (A5)$$
$$RMSE : 0.000215, \quad R^2 : 0.94$$

# References


Batool M, Cihacek LJ, Alghamdi RS (2024) Soil Inorganic Carbon Formation and the Sequestration of Secondary Carbonates in Global Carbon Pools: A Review. Soil Systems 8(1):15. https://doi.org/10.3390/soilsystems8010015

Beare M, Gregorich E, St-Georges P (2009) Compaction effects on CO2 and N2O production during drying and rewetting of soil. Soil Biology and Biochemistry 41(3):611–621. https://doi.org/10.1016/j.soilbio.2008.12.024

Berhe AA, Harte J, Harden JW, et al (2007) The Significance of the Erosion-induced Terrestrial Carbon Sink. BioScience 57(4):337–346. https://doi.org/10.1641/B570408

Berhe AA, Harden JW, Torn MS, et al (2008) Linking soil organic matter dynamics and erosion-induced terrestrial carbon sequestration at different landform positions. Journal of Geophysical Research: Biogeosciences 113(G4). https://doi.org/10.1029/2008JG000751

Berhe AA, Suttle KB, Burton SD, et al (2012) Contingency in the direction and mechanics of soil organic matter responses to increased rainfall. Plant and Soil 358(1-2):371–383. https://doi.org/10.1007/s11104-012-1156-0

Berhe AA, Barnes RT, Six J, et al (2018) Role of Soil Erosion in Biogeochemical Cycling of Essential Elements: Carbon, Nitrogen, and Phosphorus. Annual Review of Earth and Planetary Sciences 46(1):521–548. https://doi.org/10.1146/annurev-earth-082517-010018

Bird JA, Torn MS (2006) Fine Roots vs. Needles: A Comparison of 13C and 15N Dynamics in a Ponderosa Pine Forest Soil. Biogeochemistry 79(3):361–382. https://doi.org/10.1007/s10533-005-5632-y

Chaopricha NT (2013) The Importance, Origin, Composition, and Stability of Deeply Buried Soil Organic Matter. PhD thesis, University of Wisconsin-Madison, Madison

Chaopricha NT, Marín-Spiotta E (2014) Soil burial contributes to deep soil organic carbon storage. Soil Biology and Biochemistry 69:251–264. https://doi.org/10.1016/j.soilbio.2013.11.011

Chowdhury N, Marschner P, Burns RG (2011) Soil microbial activity and community composition: Impact of changes in matric and osmotic potential. Soil Biology and Biochemistry 43(6):1229–1236. https://doi.org/10.1016/j.soilbio.2011.02.012

Cotrufo MF, Lavallee JM (2025) Incorporating aridity in soil carbon stewardship frameworks. Nature Climate Change 15(3):240–242. https://doi.org/10.1038/s41558-025-02270-9

Davidson EA, Samanta S, Caramori SS, et al (2012) The ¡scp¿D¡/scp¿ ual ¡scp¿A¡/scp¿ rrhenius and ¡scp¿M¡/scp¿ ichaelis– ¡scp¿M¡/scp¿ enten kinetics model for decomposition of soil organic matter at hourly to seasonal time scales. Global Change Biology 18(1):371–384. https://doi.org/10.1111/j.1365-2486.2011.02546.x

Dolui M, Nel T, Phillips LM, et al (2026) Composition and persistence of soil organic matter along eroding and depositional transects in buried vs. modern soil layers: A case of the Brady paleosol at Wauneta, Nebraska. Geoderma 465:117660. https://doi.org/10.1016/j.geoderma.2025.117660

Elzhov T, Mullen K, Spiess A, et al (2023) minpack.lm: R Interface to the Levenberg-Marquardt Nonlinear Least-Squares Algorithm Found in MINPACK, Plus Support for Bounds. URL https://CRAN.R-project.org/package=minpack.lm.

Fierer N, Schimel JP (2003) A Proposed Mechanism for the Pulse in Carbon Dioxide Production Commonly Observed Following the Rapid Rewetting of a Dry Soil. Soil Science Society of America Journal 67(3):798. https://doi.org/10.2136/sssaj2003.0798

Fontaine S, Barot S, Barré P, et al (2007) Stability of organic carbon in deep soil layers controlled by fresh carbon supply. Nature 450(7167):277–280. https://doi.org/10.1038/nature06275

Gao X, Huang R, Li J, et al (2020) Temperature induces soil organic carbon mineralization in urban park green spaces, Chengdu, southwestern China: Effects of planting years and vegetation types. Urban Forestry & Urban Greening 54:126761. https://doi.org/10.1016/j.ufug.2020.126761

Ghezzehei TA, Sulman B, Arnold CL, et al (2019) On the role of soil water retention characteristic on aerobic microbial respiration. Biogeosciences 16(6):1187–1209. https://doi.org/10.5194/bg-16-1187-2019

Goebel MO, Bachmann J, Woche SK, et al (2005) Soil wettability, aggregate stability, and the decomposition of soil organic matter. Geoderma 128(1-2):80–93. https://doi.org/10.1016/j.geoderma.2004.12.016

Griffiths BS, Philippot L (2013) Insights into the resistance and resilience of the soil microbial community. FEMS Microbiology Reviews 37(2):112–129. https://doi.org/10.1111/j.1574-6976.2012.00343.x

Hicks Pries CE, Castanha C, Porras RC, et al (2017) The whole-soil carbon flux in response to warming. Science 355(6332):1420–1423. https://doi.org/10.1126/science.aal1319

Hicks Pries CE, Ryals R, Zhu B, et al (2023) The Deep Soil Organic Carbon Response to Global Change. Annual Review of Ecology, Evolution, and Systematics 54(1):375–401. https://doi.org/10.1146/annurev-ecolsys-102320-085332

Hill RL, Horton R, Cruse RM (1985) Tillage Effects on Soil Water Retention and Pore Size Distribution of Two Mollisols. Soil Science Society of America Journal 49(5):1264–1270. https://doi.org/10.2136/sssaj1985.03615995004900050039x

Horne D, McIntosh J (2000) Hydrophobic compounds in sands in New Zealand—extraction, characterisation and proposed mechanisms for repellency expression. Journal of Hydrology 231-232:35–46. https://doi.org/10.1016/S0022-1694(00)00181-5

IPCC (2018) Global Warming of 1.5°C. In: Masson-Delmotte V, Zhai P, Pörtner HO, et al (eds) An IPCC Special Report on the impacts of global warming of 1.5°C above pre-industrial levels and related global greenhouse gas emission pathways, in the context of strengthening the global response to the threat of climate change. Intergovernmental Panel on Climate Change., https://doi.org/10.1038/291285a0

Jacobs PM, Mason JA (2004) Paleopedology of soils in thick Holocene loess, Nebraska, USA. Revista Mexicana de Ciencias Geológicas 21(1):54–70

Jacobs PM, Mason JA (2007) Late Quaternary climate change, loess sedimentation, and soil profile development in the central Great Plains: A pedosedimentary model. Geological Society of America Bulletin 119(3-4):462–475. https://doi.org/10.1130/B25868.1

Jobbagy EG, Jackson RB (2000) The Vertical Distribution of Soil Organic Carbon and Its Relation to Climate and Vegetation. Ecological Applications 10(2):423–436

Johnson WC, Willey KL (2000) Isotopic and rock magnetic expression of environmental change at the Pleistocene–Holocene transition in the central Great Plains. Quaternary International 67(1):89–106. https://doi.org/10.1016/S1040-6182(00)00011-2

Johnson WC, Willey KL, Mason JA, et al (2007) Stratigraphy and environmental reconstruction at the middle Wisconsinan Gilman Canyon formation type locality, Buzzard's Roost, southwestern Nebraska, USA. Quaternary Research 67(3):474–486. https://doi.org/10.1016/j.yqres.2007.01.011

Kaiser M, Kleber M, Berhe AA (2015) How air-drying and rewetting modify soil organic matter characteristics: An assessment to improve data interpretation and inference. Soil Biology and Biochemistry 80:324–340. https://doi.org/10.1016/j.soilbio.2014.10.018

Kang S, Xing B (2008) Humic Acid Fractionation upon Sequential Adsorption onto Goethite. Langmuir 24(6):2525–2531. https://doi.org/10.1021/la702914q

Kemper WD, Rosenau RC, Dexter AR (1987) Cohesion Development in Disrupted Soils as Affected by Clay and Organic Matter Content and Temperature. Soil Science Society of America Journal 51(4):860–867. https://doi.org/10.2136/sssaj1987.03615995005100040004x

Leizeaga A, Hicks LC, Manoharan L, et al (2021) Drought legacy affects microbial community trait distributions related to moisture along a savannah grassland precipitation gradient. Journal of Ecology 109(9):3195–3210. https://doi.org/10.1111/1365-2745.13550

Lenth RV (2024) emmeans: Estimated Marginal Means, aka Least-Squares Means. URL https://CRAN.R-project.org/package=emmeans

Li Q, Hu W, Li L, et al (2023) Interactions between organic matter and Fe oxides at soil micro-interfaces: Quantification, associations, and influencing factors. Science of The Total Environment 855:158710. https://doi.org/10.1016/j.scitotenv.2022.158710

Liu T, Wang L, Feng X, et al (2018) Comparing soil carbon loss through respiration and leaching under extreme precipitation events in arid and semiarid grasslands. Biogeosciences 15(5):1627–1641. https://doi.org/10.5194/bg-15-1627-2018

Marin-Spiotta E, Chadwick OA, Kramer M, et al (2011) Carbon delivery to deep mineral horizons in Hawaiian rain forest soils. Journal of Geophysical Research 116(G3):G03011. https://doi.org/10.1029/2010JG001587

Marin-Spiotta E, Chaopricha NT, Plante AF, et al (2014) Long-term stabilization of deep soil carbon by fire and burial during early Holocene climate change. Nature Geoscience 7(6):428–432. https://doi.org/10.1038/ngeo2169

Mason JA, Jacobs PM, Hanson PR, et al (2003) Sources and paleoclimatic significance of Holocene Bignell Loess, central Great Plains, USA. Quaternary Research 60(3):330–339. https://doi.org/10.1016/j.yqres.2003.07.005

Mason JA, Miao X, Hanson PR, et al (2008) Loess record of the Pleistocene–Holocene transition on the northern and central Great Plains, USA. Quaternary Science Reviews 27(17-18):1772–1783. https://doi.org/10.1016/j.quascirev.2008.07.004

McDowell T (2020) Processes controlling soil hydrology and pedogenic carbonate formation in loess tablelands, Nebraska, USA. PhD thesis, University of Wisconsin-Madison, Madison

McDowell TM, Mason JA, Vo T, et al (2022) Hydrology of a Semiarid Loess-Paleosol Sequence, and Implications for Buried Soil Connection to the Modern Climate, Plant-Available Moisture, and Loess Tableland Persistence. Journal of Geophysical Research: Earth Surface 127(12). https://doi.org/10.1029/2022JF006800

McMurtry AR, Kasmerchak CS, Vaughan EA, et al (2024) Getting to the root of the problem: Soil carbon and microbial responses to root inputs within a buried paleosol along an eroding hillslope in southwestern Nebraska, USA. Soil Biology and Biochemistry 198:109549. https://doi.org/10.1016/j.soilbio.2024.109549

Miao X, Mason JA, Swinehart JB, et al (2007) A 10,000 year record of dune activity, dust storms, and severe drought in the central Great Plains. Geology 35(2):119. https://doi.org/10.1130/G23133A.1

Miller A, Schimel J, Meixner T, et al (2005) Episodic rewetting enhances carbon and nitrogen release from chaparral soils. Soil Biology and Biochemistry 37(12):2195–2204. https://doi.org/10.1016/j.soilbio.2005.03.021

Min K, Berhe AA, Khoi CM, et al (2020) Differential effects of wetting and drying on soil CO2 concentration and flux in near-surface vs. deep soil layers. Biogeochemistry 148(3):255–269. https://doi.org/10.1007/s10533-020-00658-7

Najera F, Dippold MA, Boy J, et al (2020) Effects of drying/rewetting on soil aggregate dynamics and implications for organic matter turnover. Biology and Fertility of Soils 56(7):893–905. https://doi.org/10.1007/s00374-020-01469-6

Naorem A, Jayaraman S, Dalal RC, et al (2022) Soil Inorganic Carbon as a Potential Sink in Carbon Storage in Dryland Soils—A Review. Agriculture 12(8):1256. https://doi.org/10.3390/agriculture12081256

Neff JC, Asner GP (2001) Dissolved Organic Carbon in Terrestrial Ecosystems: Synthesis and a Model. Ecosystems 4(1):29–48. https://doi.org/10.1007/s100210000058

Or D, Tuller M (1999) Liquid retention and interfacial area in variably saturated porous media: Upscaling from single-pore to sample-scale model. Water Resources Research 35(12):3591–3605. https://doi.org/10.1029/1999WR900262

Pal SC, Chakrabortty R, Towfiqul Islam ARM, et al (2023) Land use and climate change-induced soil erosion mapping in a sub-tropical environment. Geomatics, Natural Hazards and Risk 14(1). https://doi.org/10.1080/19475705.2023.2270129

Pausch J, Loeppmann S, Kühnel A, et al (2016) Rhizosphere priming of barley with and without root hairs. Soil Biology and Biochemistry 100:74–82. https://doi.org/10.1016/j.soilbio.2016.05.009

Pinheiro J, Bates D, DebRoy S, et al (2024) nlme: Linear and Nonlinear Mixed Effects Models. URL https://CRAN.R-project.org/package=nlme

R Core Team (2025) R: A Language and Environment for Statistical Computing. URL https://www.r-project.org/

RStudio Team (2019) RStudio: Integrated Development for R. RStudio. URL http://www.rstudio.com/

Rumpel C, Kögel-Knabner I (2011) Deep soil organic matter—a key but poorly understood component of terrestrial C cycle. Plant and Soil 338(1-2):143–158. https://doi.org/10.1007/s11104-010-0391-5

Schmidt MWI, Torn MS, Abiven S, et al (2011) Persistence of soil organic matter as an ecosystem property. Nature 478(7367):49–56. https://doi.org/10.1038/nature10386

Schrumpf M, Kaiser K, Guggenberger G, et al (2013) Storage and stability of organic carbon in soils as related to depth, occlusion within aggregates, and attachment to minerals. Biogeosciences 10(3):1675–1691. https://doi.org/10.5194/bg-10-1675-2013

Sharififar A, Minasny B, Arrouays D, et al (2023) Soil inorganic carbon, the other and equally important soil carbon pool: Distribution, controlling factors, and the impact of climate change. p 165–231, https://doi.org/10.1016/bs.agron.2022.11.005

Six J, Conant R, Paul E, et al (2002) Review: Stabilization Mechanisms of Soil Organic Matter: Implications for C-Saturation of Soils. Plant and Soil 241(2):155–176

Soong JL, Castanha C, Hicks Pries CE, et al (2021) Five years of whole-soil warming led to loss of subsoil carbon stocks and increased CO ¡sub¿2¡/sub¿ efflux. Science Advances 7(21). https://doi.org/10.1126/sciadv.abd1343

Stacy EM, Hart SC, Hunsaker CT, et al (2015) Soil carbon and nitrogen erosion in forested catchments: implications for erosion-induced terrestrial carbon sequestration. Biogeosciences 12(16):4861–4874. https://doi.org/10.5194/bg-12-4861-2015

Steenwerth K, Jackson L, Calderon F, et al (2005) Response of microbial community composition and activity in agricultural and grassland soils after a simulated rainfall. Soil Biology and Biochemistry 37(12):2249–2262. https://doi.org/10.1016/j.soilbio.2005.02.038

Szymanski LM (2021) Spatial Distribution and Long-Term Persistence of Ancient Carbon in Buried Soils and Its Vulnerability to Landscape Disturbance. PhD thesis, University of Wisconsin-Madison, Madison

Tsypin M, Macpherson G (2012) The effect of precipitation events on inorganic carbon in soil and shallow groundwater, Konza Prairie LTER Site, NE Kansas, USA. Applied Geochemistry 27(12):2356–2369. https://doi.org/10.1016/j.apgeochem.2012.07.008

Venables WN, Ripley BD (2002) MASS (Modern Applied Statistics with S). URL https://CRAN.R-project.org/package=MASS

Wahab LM, Kim S, Berhe AA (2025) Carbon and Nitrogen Dynamics in Subsoils After 20 years of Added Precipitation in a Mediterranean Grassland. https://doi.org/10.5194/egusphere-2024-3607

Xiang SR, Doyle A, Holden PA, et al (2008) Drying and rewetting effects on C and N mineralization and microbial activity in surface and subsurface California grassland soils. Soil Biology and Biochemistry 40(9):2281–2289. https://doi.org/10.1016/j.soilbio.2008.05.004

Zhu B, Cheng W (2013) Impacts of drying–wetting cycles on rhizosphere respiration and soil organic matter decomposition. Soil Biology and Biochemistry 63:89–96. https://doi.org/10.1016/j.soilbio.2013.03.027